

# SANDIA REPORT

SAND2010-7318

Unlimited Release

Printed September 2010

## Scaling of X pinches from 1 MA to 6 MA

Daniel B. Sinars<sup>1</sup>, Ryan D. McBride<sup>1</sup>, David F. Wenger<sup>1</sup>, Michael E. Cuneo<sup>1</sup>,  
Edmund P. Yu<sup>1</sup>, Eric Harding<sup>1</sup>, Stephanie B. Hansen<sup>1</sup>, David J. Ampleford<sup>1</sup>,  
Chris A. Jennings<sup>1</sup>, Sergei A. Pikuz<sup>2</sup>, Tatiana A. Shelkovenko<sup>2</sup>, Jeremy P. Chittenden<sup>3</sup>,  
Simon N. Bland<sup>3</sup>

<sup>1</sup> Sandia National Laboratories, P.O. Box 5800, Albuquerque, NM 87185, USA

<sup>2</sup> Laboratory of Plasma Studies, Cornell University, Ithaca, NY 14853, USA

<sup>3</sup> Blackett Laboratory, Imperial College, London SW7 2BW, United Kingdom

Prepared by  
Sandia National Laboratories  
Albuquerque, New Mexico 87185 and Livermore, California 94550

Sandia National Laboratories is a multi-program laboratory managed and operated by Sandia Corporation, a wholly owned subsidiary of Lockheed Martin Corporation, for the U.S. Department of Energy's National Nuclear Security Administration under contract DE-AC04-94AL85000.

Approved for public release; further dissemination unlimited.

Issued by Sandia National Laboratories, operated for the United States Department of Energy by Sandia Corporation.

**NOTICE:** This report was prepared as an account of work sponsored by an agency of the United States Government. Neither the United States Government, nor any agency thereof, nor any of their employees, nor any of their contractors, subcontractors, or their employees, make any warranty, express or implied, or assume any legal liability or responsibility for the accuracy, completeness, or usefulness of any information, apparatus, product, or process disclosed, or represent that its use would not infringe privately owned rights. Reference herein to any specific commercial product, process, or service by trade name, trademark, manufacturer, or otherwise, does not necessarily constitute or imply its endorsement, recommendation, or favoring by the United States Government, any agency thereof, or any of their contractors or subcontractors. The views and opinions expressed herein do not necessarily state or reflect those of the United States Government, any agency thereof, or any of their contractors.

Printed in the United States of America. This report has been reproduced directly from the best available copy.

Available to DOE and DOE contractors from  
U.S. Department of Energy  
Office of Scientific and Technical Information  
P.O. Box 62  
Oak Ridge, TN 37831

Telephone: (865) 576-8401  
Facsimile: (865) 576-5728  
E-Mail: [reports@adonis.osti.gov](mailto:reports@adonis.osti.gov)  
Online ordering: <http://www.osti.gov/bridge>

Available to the public from  
U.S. Department of Commerce  
National Technical Information Service  
5285 Port Royal Rd.  
Springfield, VA 22161

Telephone: (800) 553-6847  
Facsimile: (703) 605-6900  
E-Mail: [orders@ntis.fedworld.gov](mailto:orders@ntis.fedworld.gov)  
Online order: <http://www.ntis.gov/help/ordermethods.asp?loc=7-4-0#online>



## Scaling of X pinches from 1 MA to 6 MA

Daniel B. Sinars, Ryan D. McBride, David F. Wenger, Michael E. Cuneo, Edmund P. Yu,  
Eric Harding, Stephanie B. Hansen, David J. Ampleford, Chris A. Jennings

Radiation and Fusion Experiments  
Sandia National Laboratories  
P.O. Box 5800  
Albuquerque, New Mexico 87185, USA

Sergei A. Pikuz, Tatiana A. Shelkovenko  
Laboratory of Plasma Studies  
Cornell University  
Ithaca, New York 14853, USA

Jeremy P. Chittenden, Simon N. Bland  
Blackett Laboratory  
Imperial College  
London SW7 2BW, United Kingdom

### Abstract

This final report for Project 117863 summarizes progress made toward understanding how X-pinch load designs scale to high currents. The X-pinch load geometry was conceived in 1982 as a method to study the formation and properties of bright x-ray spots in z-pinch plasmas. X-pinch plasmas driven by 0.2 MA currents were found to have source sizes of 1 micron, temperatures  $>1$  keV, lifetimes of 10-100 ps, and densities  $>0.1$  times solid density. These conditions are believed to result from the direct magnetic compression of matter. Physical models that capture the behavior of 0.2 MA X pinches predict more extreme parameters at currents  $>1$  MA. This project developed load designs for up to 6 MA on the SATURN facility and attempted to measure the resulting plasma parameters. Source sizes of 5-8 microns were observed in some cases along with evidence for high temperatures (several keV) and short time durations ( $<500$  ps).

## **ACKNOWLEDGMENTS**

This work was funded in part by Laboratory-Directed Research and Development funds at Sandia National Laboratories. The authors would like to thank Dr. Mark Herrmann for encouragement in proposing this work for Sandia LDRD support. The authors would also like to thank the Science of Extreme Environments (SEE) LDRD committee for their support of this research. The authors would also like to acknowledge the dedicated and professional SATURN operations crew led by Ken Mikkelsen and Brad Peyton whose efforts made this LDRD possible.

# CONTENTS

1. Motivation and scope of Project .....	9
2. Discussion of the Main Challenges Addressed by the Project .....	11
2.1 How to design a 3-6 MA X-pinch load?.....	11
2.2 How to diagnose the micro-pinch plasma parameters? .....	14
3. Description of the Experimental setup and methods .....	17
3.1 SATURN Power Feed Hardware.....	17
3.2 X-pinch Target Hardware .....	19
3.3 Diagnostic Description.....	23
3.3.1 X-ray power and energy measurements .....	23
3.3.2 X-ray imaging measurements.....	29
3.3.3 X-ray spot size measurements .....	31
3.3.4 X-ray streak camera measurements.....	38
3.3.5 X-ray spectroscopy measurements .....	44
4. Discussion of Key Experimental Results.....	47
5. Project Accomplishments .....	49
6. Ideas for Future Work.....	51
7. Project Significance and Conclusions.....	53
References.....	54
Distribution .....	55

## FIGURES

Figure 1: Example load photographs of X-pinch configurations tested during this project. (a) Pre-installation photograph of the 128-wire X-pinch array load used on s3734, along with (b) a close-in view of its cross-point. (c) A view of the nested X-pinch tested on s3767. (d) A view of the solid tungsten X pinch tested on s3770.....	13
Figure 2: A conceptual illustration of a nested X pinch. (a) Nested cylindrical wire arrays of different radii are rotated to produce (b) optimal packing at the resulting cross point.....	13
Figure 3: Cross-section of wire-array X-pinch SATURN power feed hardware (A0019 only). Note that this hardware set used the large-diameter convolute. ....	18
Figure 4: Cross-Section of Solid X-pinch SATURN power feed hardware (A0035; A0047; A0076; A0110; A0141). Note that this hardware used the small-diameter convolute. The first four hardware sets in A0035 used a wire-array X-pinch target in place of the solid X-pinch hardware shown. The last two hardware sets in A0035 used a solid X-pinch target as shown, but the target X-pinch height in those targets matched the taller height of the wire-array X-pinch targets as discussed in Section 2.2 .....	18
Figure 5: Dimensions of the high-number wire-array X-pinch targets (A0019).....	19
Figure 6: Dimensions of the nested wire-array X-pinch targets (A0035). ....	20
Figure 7: Drawing of the tall solid X-pinch targets (A0035). The target dimensions are identical to those of the nested wire-array X-pinch targets. ....	20
Figure 8: Dimensions of the compact solid X-pinch targets (A0047, A0076, A0110, A0141). ..	21
Figure 9: Diagram illustrating the view of the X-pinch cross-point as seen from one of the LOS diagnostics. This extreme viewing angle constrained the load hardware design. ....	21
Figure 10: Plot of PCD Filter Transmission vs. Photon Energy.....	23
Figure 11: Example radiation powers for selected X-pinch tests. The columns show data from solid Cu/Ni, W/Cu, and W X-pinch loads, respectively. The rows show the total soft (~0.1-1 keV) x-ray power, the >1 keV x-ray power, and the 3-5 keV x-ray power, respectively. Based on the MLM images, the total power is believed to come from a height of ~3 mm. ....	28
Figure 12: Photo of LOS B. The MLM instrument is the square cross-section piece with the honeycomb structure. The XRDs were located on the pipe above the MLM.....	30
Figure 13: Example MLM data from s3814 (solid Cu/Ni X pinch) .....	30
Figure 14: Schematic diagram of slit camera designed for the first SATURN shot series (s3734-3737). The design was abandoned because x-ray diffraction was limiting the source size determination to ~20 microns. ....	31
Figure 15: Cross-section of the in-chamber high-magnification slit camera used to measure the x-ray spot size.....	32
Figure 16: Photo of SATURN center section showing the slit camera (to the left of the author) and the time-integrated convex crystal spectrometer (above author). ....	32
Figure 17: Plot of HMSC filter transmissions versus photon energy for all filters used during the course of this project.....	33
Figure 18: Plot of HMSC filter transmission vs. photon energy for one of the most common configurations for which data was obtained. ....	34
Figure 19: Example high-magnification slit camera data (LOS version) from s3769, a solid tungsten X-pinch load. The entire film is shown in (a), along with expanded views of the Cu-filtered (b) horizontal and (c) vertical slits. Looking carefully at the two sets of slit images, one	

can see that two relatively small x-ray sources were produced, displaced mainly vertically from one another. From the data we can determine that the sources were separated by 32 microns along the vertical direction. A lineout through the 20-micron slit data is shown in (d), in which it can be seen that the edge is approximately 28 microns wide. Much of this may be due to diffraction effects, which is estimated to blur a sharp edge to  $\sim 21$  microns at the distances used in this diagnostic. .... 35

Figure 20: Example high-magnification slit camera data (center section version) from s3941, a solid tungsten X-pinch load. The entire film is shown in (a), along with expanded views of the Cu-filtered (b) horizontal and (c) vertical slits. In this case one small-diameter source was produced and a second, more intense but larger-size source was also produced that was shifted about 177 microns horizontally. The diagonal variations in the intensity from the upper left to the lower right are caused by imperfect slit filter alignments. On this test an 18.5-micron diameter stainless steel wire was strung across the bottom slits, as shown in an expanded view in (d). .... 36

Figure 21: Lineouts through the Cu-filtered slit data from s3941, a solid tungsten X-pinch load. The second, larger-diameter source made it difficult to extract the sharper image. Two lineouts through the image were made, shown in part (a), and are plotted in (b). The lineouts were subtracted to produce the plot shown in (c). The 10-90% edge distances are measured in parts (d) and (e), and are 5.2 and 7.6 microns, respectively. .... 37

Figure 22: View of SATURN vacuum chamber from the end of LOS C. The vacuum chamber ports can be seen inside the circular ring in the background. The connection point of LOS B can be seen to the upper left. The x-ray streak camera mounted on LOS C is seen in the foreground. .... 39

Figure 23: Photo of the x-ray streak camera diagnostic as installed at the end of LOS C. A fast-closing valve was used at the end of the pipe to isolate the streak camera from debris and the post-shot rise in vacuum pressure. A polyimide filter was installed between the fast valve and turbo pump. An angle was placed just in front of the streak camera body to eliminate a direct line of sight down the pipe to the streak camera phosphor screen. The electronics controlling the streak camera and its micro-channel plate detector went through shielded cable into the large copper screen-box in the background. The streak camera body was shielded from magnetic fields using two pieces of mu-metal shielding held against the body by two white tie wraps. The author (DBS) is shown in the foreground. .... 40

Figure 24: Example x-ray streak camera data from selected experiments. (a) Data taken at speed 2 from s3859, a solid W/Cu X pinch, also shown in (b) with the 12 different filter labels superimposed over the image. (c) Data taken at speed 3 from s3860, a solid W/Cu X pinch. (d) Data taken at speed 2 from s3944, a solid W X pinch. .... 41

Figure 25: A comparison between the x-ray streak camera and PCD data from s3859, a solid W/Cu X-pinch load. The 7.0- and 12.5-micron Ti-filtered streak data fairly closely resembles the Ti-filtered PCD trace (signal PATi12138). The first x-ray burst in this experiment contained very hard radiation  $>6$  keV that was seen in the Ni-, Cu-, and Zn-filtered portions of the streak. .... 42

Figure 26: Hard ( $>6$  keV) x-ray time duration from s3859 measured using the x-ray streak camera. Also shown in red is the estimated streak response function, estimated by convolving a 120-micron-wide square wave (the slit image) with a 100-micron FWHM Gaussian (representing the MCP spatial resolution). This is optimistic in that it assumes perfect focusing, which was not always maintained during the experiments. Subtracting the streak response function in quadrature gives FWHMs for the polyimide-, Ni-, Cu-, and Zn-filtered regions of 0.51, 0.42, 0.39, and 0.42 ns, respectively. .... 43

Figure 27: Selected streak camera lineouts compared with Ti-filtered PCD data from s3944, a solid W X-pinch load. The peak at 248.4 ns had FWHMs in the PCD and polyimide-, Al-, 7.0-micron Ti, and 12.5-micron Ti-filtered regions of 0.59, 0.44, 0.52, 0.47, and 0.56 ns, respectively. .... 43

Figure 28: Example TIXTL data from s3812 (Cu/Ni/Mn target) and a preliminary analysis. .... 46

## TABLES

Table 1: Summary of hardware used during SATURN experiments ..... 17

Table 2: Summary of the X-pinch target parameters on each shot..... 22

Table 3: Summary of the properties of the Cu/Ni, W/Cu, and Ni/Cr alloys used. .... 22

Table 4: List of PCD filters used on each shot. .... 24

Table 5: List of selected PCD peak powers and radiated energy by shot..... 25

Table 6: Bolometer radiation energy and peak power by shot. .... 26

Table 7: List of implosion parameters by shot and type. For the purposes of estimating the implosion time, the start time was defined as  $t_0 = t(2.8 \text{ MA}) - 50 \text{ ns}$  (except s3898). .... 27

Table 8: Filter and film configuration for the high-magnification slit camera (HMSC). The Cu and Ti filters were each applied to only half of the slits as shown in Figure 14(a). The Kapton filters were applied to the entire image. All filter thickness are in microns. The Cu-filtered slits were always up in the real world. The films are all from Kodak..... 33

Table 9: Summary of x-ray streak camera (XRSC) diagnostic configurations and results. .... 39

Table 10: Summary of TIXTL configurations and data. .... 45

# 1. MOTIVATION AND SCOPE OF PROJECT

Experiments studying single-wire z-pinch driven by  $>100$  kA [1,2] revealed small, localized plasma constrictions which produced bright x-ray emission. In these experiments the constrictions formed at random points along the wires, which made diagnosing the plasma conditions difficult. The X pinch, first proposed by Ulshmid in 1981 during a visit to the P.N. Lebedev Physical Institute in Russia [3], provides a method for the study of these micropinch plasmas. X-pinch loads were originally created using two (or more) fine wires arranged so that they cross and touch at a single point (forming an “X” shape). The wires are placed as the load of a high current pulsed power generator (pulser). The pulser current is divided between (among) the wires except at the cross point, where all of the current is available to implode the plasma formed there during the current-induced wire explosion. Ideally the current in each leg is below the threshold for micropinch formation but at the cross point the current exceeds the threshold and these “micropinches” form reliably.

Experiments at Cornell have demonstrated that X-pinch-produced micropinches at 200 kA are 0.8-1.5 microns in diameter [4,5], have temperatures of about 1 keV, densities  $>10\%$  of solid density, and last for 10-100 ps [6,7,8], making them warm-dense objects of considerable interest. These small source sizes make the X-pinch particularly useful for high-resolution point-projection radiography (and phase contrast imaging [9]), and the Inertial Confinement Fusion community has examined their utility for measuring the uniformity of tritium ice layers in capsules [10]. For these reasons there have been numerous studies of X pinches worldwide. For example, in 2006 there were 17 publications on X pinches from five countries (U.S., Russia, China, England, and France).

A 2007 Physical Review Letter by Chittenden *et al.* briefly noted that Mo X-pinch plasmas driven by 1 MA might radiate 80 GW from a 1-micron, 10 times solid density source, and at 10 MA would radiate 3.4 TW from a 1-micron, 250x solid density source [11]. Such plasmas would be extremely interesting physical objects, and the radiation power is comparable to that produced by high-power lasers so that it may be possible to use these sources in various applications. Typical university-level facilities are 1-2 MA, and worldwide only two  $\sim 100$ -ns-class generators exist that can deliver  $>5$  MA to an inductive z-pinch load, the 6 MA SATURN and 20 MA Z pulsed power facilities at Sandia National Laboratories.

This report describes the results of X-pinch research on the 6 MA SATURN facility designed to explore the scaling of micropinch plasma conditions observed at 1 MA to higher currents and to test whether the extreme micropinch conditions suggested by Chittenden *et al.* could be realized in the laboratory. The two primary challenges faced by the project were (a) to determine what type of X-pinch load might create such conditions, and (b) to determine what the properties of any resulting micropinch plasmas were.

From 2008-2010 six experimental series totaling 31 shots were conducted on SATURN that tested a variety of X-pinch designs. Two key diagnostics were developed during the course of the experiments to measure the x-ray spot size and the time duration of the x-ray emission. The experiments succeeded in creating a continuum x-ray source in the 6-9 keV range that was 5-7 microns in diameter. The experiments also demonstrated that this high-energy emission is

typically emitted in a time  $<0.5$  ns in duration. The final experiments were conducted in August 2010, shortly before the preparation of this report. As a result much of the data is still being analyzed at the time of this report. The report summarizes the experimental configurations tested, the methods and diagnostics developed during this project, and some of the key early findings of the data analysis. The report will provide useful background for a refereed journal publication on the results of these experiments. The report concludes with some recommendations for future follow-on work and opportunities provided by this research.

## 2. DISCUSSION OF THE MAIN CHALLENGES ADDRESSED BY THE PROJECT

### 2.1 How to design a 3-6 MA X-pinch load?

The first major problem faced by this project was to determine what the optimum X-pinch geometry and mass per unit should be. A 2006 review of X-pinch research in the literature showed that all of the work done on X pinches worldwide had been done at current levels of 1.0 MA or less, with the vast majority at current levels  $<0.5$  [12]. It was not clear that the 1.0 MA experiments up to that point had been optimized, since they used similar parameters to lower-current X pinches. For experiments  $<0.5$  MA, X pinches composed of 2-4 wires were used, with wire diameters that were typically 25 microns or less. The optimum configuration for each generator was determined empirically, since even to this day these loads are extremely challenging to model quantitatively.

To better understand how to design a high-current X-pinch load, many of the project researchers were involved in early scaling experiments on the 1 MA COBRA facility at Cornell University. This initial work was conducted in 2007 and funded in part by a previous LDRD, "High Power Density X-ray Sources." The goal of the experiments was to explore the behavior of X pinches with higher mass per unit length, with an eye toward evaluating possible issues with X pinches designed for 3-6 MA. The x-ray source size and radiation power of 1 MA X pinches were studied as a function of wire material (Al, Ti, Mo, and W) and wire number (1-, 2-, 8-, 32-, and 64-wire configurations). In those initial experiments, the smallest bright spots observed were from 32-wire tungsten X pinches, which produced  $\sim 11$ - $16 \mu\text{m}$ ,  $\sim 2$  J, 1-10 GW sources of 3-5 keV continuum radiation [24].

The early 1 MA X-pinch research revealed some unforeseen surprises. First, it was found that X pinches composed of large-diameter wires ( $d > 50 \mu\text{m}$ ) appeared to behave differently than X pinches made with smaller diameter wires. Most notably, the large-diameter wires appeared to expand to a very large extent, which may have affected the ability of a small-diameter z-pinch to form at the cross-point. Second, it was found that arrays with large numbers of wires did not always form a compact, uniformly distributed grouping of wires at the cross point. Third, an attempt was made to use a single large-diameter wire strung across two solid Al cones as the ultimate limit of a perfectly cylindrically symmetric X pinch and a precursor to an idea for how to build a 3-6 MA X pinch. Those experiments failed badly, in part we now believe because of the use of Al cones rather than a high-Z material like tungsten.

The initial assumption was that the mass per unit length of the X pinch should scale roughly as the square of the current. Work at 0.4 MA successfully used a 4 by 25- $\mu\text{m}$  W X-pinch that was about 0.38 mg/cm. The 1 MA X-pinch experiments at Cornell studied X pinches of 1.5 and 3.0 mg/cm [24]. The 3 mg/cm loads generally resulted in the first x-ray burst occurring just before the peak of the current, near 1-1.2 MA. The 1.5 mg/cm arrays pinched slightly earlier at a current of about 0.7 MA. The exception was the 2-wire X pinches, possibly because of the extremely large wire expansion noted above.

As a result of the previous 1 MA work, the initial experiments for SATURN proposed to study mainly high wire-number W X pinches with a relatively large mass of 108 mg/cm. The baseline design was a 128 by 75- $\mu\text{m}$  W X-pinch load. Despite the high wire number, the wire diameter at this large mass per unit length was very large and there was concern about whether the wires would expand to large diameters as in the 1 MA experiments. What we overlooked was that since we could not adjust the density, as we increased the mass per unit length of the X pinch we were also substantially increasing the diameter of the cross point region and thus reducing the magnetic pressure. In retrospect, it was perhaps not surprising that the 108 mg/cm load pinched extremely late in the SATURN current pulse and performed very badly. During the first experiments we continued to reduce the wire number and wire diameter of the tungsten until we reached a 32 by 53- $\mu\text{m}$  W X-pinch load with 13.6 mg/cm, which pinched before the peak of the current.

After the experiments, the team considered the scaling used to design wire-array z-pinches. To scale a wire array implosion self-similarly to different conditions, the parameter P should be fixed, where

$$\Pi = (\mu_0 I^2 \tau^2) / (4 \pi m l r^2),$$

and I is the peak current,  $\tau$  is the rise time of the current, ml is the mass per unit length, and r is the radius of the wire array [27]. In a wire array, the mass per unit length can normally be changed arbitrarily by increasing the number of wires in the array with changing the array radius. In the case of X pinches, where the mass is initially all on the axis to start with and the density is a fixed property of the wire material, the mass per unit length and the radius are linked. Substituting the relationship  $ml = \rho \pi r^2$ , we arrive at the following scaling relation,

$$(I_1^2 \tau_1^2) / (\rho_1 r_1^4) = (I_2^2 \tau_2^2) / (\rho_2 r_2^4).$$

Using approximate parameters for the 3 mg/cm tungsten COBRA X pinches,  $I=1.0$  MA,  $\tau=70$  ns,  $\rho=19.3$  g/cm<sup>3</sup>,  $r\sim 3.5*25$   $\mu\text{m}$  (assuming a close-packed 32-wire array), and representative parameters for SATURN's small-diameter convolute in short-pulse mode,  $I=5.5$  MA,  $\tau=50$  ns,  $\rho=19.3$  g/cm<sup>3</sup>, one can estimate the radius of the optimum tungsten X pinch as about 173  $\mu\text{m}$ , which corresponds to a mass per unit length of 18.1 mg/cm. This is not too far from the 13.6 mg/cm that empirically appeared to work during the first SATURN experimental series and far less than the originally estimated 108 mg/cm based only on  $I^2$ .

One of the problems with high wire-number arrays on SATURN was the packing of the wires at the cross point. Depending on how well the wires came together, the outer radius of the array could vary. Also, due to the angle of the wires, the wire cross-sections in the plane of the cross point are no longer circular, making it difficult to control and accurately know the initial conditions of the X-pinch cross point. An example photograph of the 128-wire experiment is shown in Figure 1, in which it is clear that the cross point is rather complex. Continued experiments at Cornell's 1 MA facility had demonstrated that through a proper choice of array and wire diameters, an X pinch could be constructed from a nested wire array system to give nearly optimum packing [28], as illustrated in Figure 2. This idea was explored during the second experimental shot series on SATURN. The idea of a solid, machined cross-point region was also explored again during the second experimental series using tungsten, despite the earlier failure on the COBRA facility. The series focused on loads with mass per unit lengths of 13-18 mg/cm, close to the 13.6 mg/cm empirically determined during the first series.

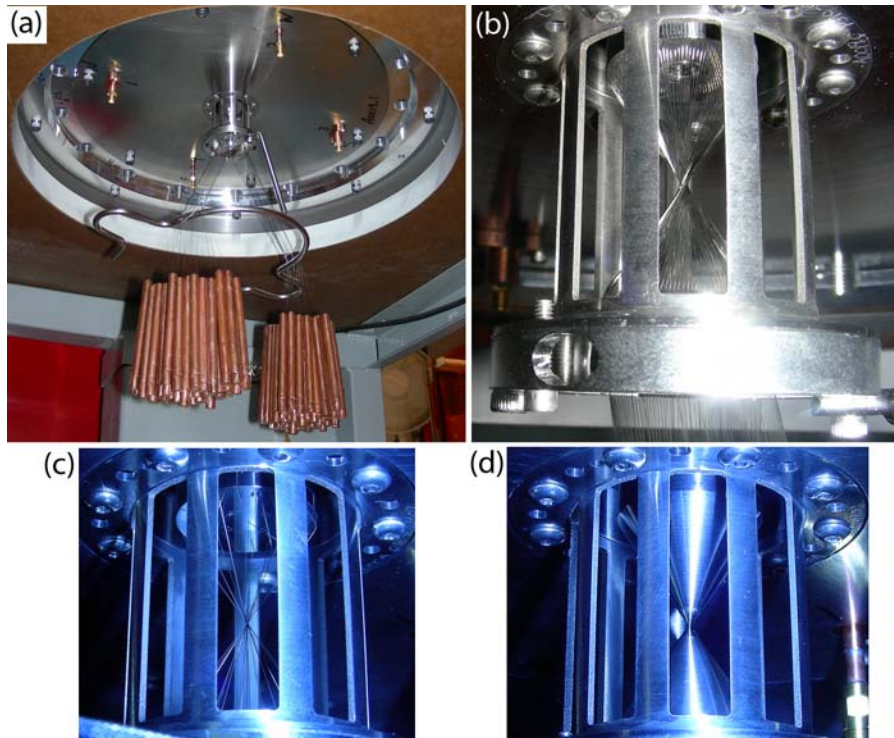


**Figure 1: Example load photographs of X-pinch configurations tested during this project. (a) Pre-installation photograph of the 128-wire X-pinch array load used on s3734, along with (b) a close-in view of its cross-point. (c) A view of the nested X-pinch tested on s3767. (d) A view of the solid tungsten X pinch tested on s3770.**

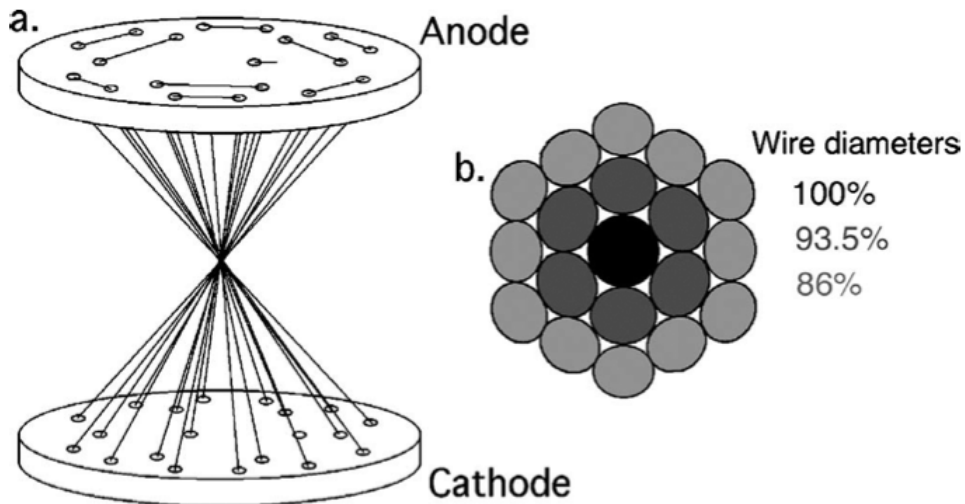


**Figure 2: A conceptual illustration of a nested X pinch. (a) Nested cylindrical wire arrays of different radii are rotated to produce (b) optimal packing at the resulting cross point.**

The “solid” X pinches tested during the second experimental series worked the best of any of the load configurations tried up to that point. Though nested arrays offered some advantages in terms of being able to mix wire materials, thereby providing a way to insert other materials for spectroscopy or further load optimization, solid X pinches appeared to offer the best opportunity

for reproducibility and the loads were comparatively easy to fabricate and install. For this reason, all of the remaining experiments on SATURN used solid X pinches, rather than wire-array-based X pinches. Future experiments could consider revisiting the use of nested X pinches, as considerable experience has been developed with these loads on the 1 MA COBRA facility in the meantime.

Having achieved some measure of success with solid tungsten X pinches, the next few experimental series attempted to develop improved diagnostics to measure the plasma parameters as discussed in the next section. As such, solid X pinches composed of various alloys were explored. With the emphasis on improving the measurements, it was only belatedly realized that the loads were generally producing their first x-ray bursts in the 3-4 MA range rather than closer to peak current, near 5-6 MA. Also, it was found that the smallest x-ray spot sizes appeared to be produced mainly from the pure tungsten X pinches rather than alloys of lower-Z materials, the possible exception being the W/Cu alloy. As a result, the final experimental series focused on pure tungsten X pinches of varying diameters up to 23.8 mg/cm ( $r = 198 \mu\text{m}$ ), increased from the 14.1 mg/cm ( $r = 153 \mu\text{m}$ ) tested originally. Despite the larger mass and lower magnetic pressure, the time of the first x-ray bursts still did not reach the desired 5-6 MA range. As such, it is not clear whether the optimal mass per unit length may not still be larger than what we tested during this project. Should additional work of this type continue in the future, we strongly recommend that larger mass per unit length solid tungsten X pinches be investigated.

## 2.2 How to diagnose the micro-pinch plasma parameters?

The second significant challenge faced by the project was to measure the parameters of the x-ray sources and plasmas produced on SATURN experiments. SATURN was originally designed as a high-energy ( $>100 \text{ keV}$ ) bremsstrahlung source, and as such the diagnostic ports needed for low-energy ( $0.1\text{-}10 \text{ keV}$ ) research were added later. SATURN possesses the basic diagnostic suite for low-energy z-pinch measurements: x-ray power and energy diagnostics and a time-gated x-ray pinhole camera diagnostic. The experimenter must supply any additional diagnostics.

The most important two parameters to measure are the x-ray source size of the continuum x-ray radiation and the time duration of the x-ray radiation. The most extreme plasma parameters in 0.2 MA experiments occurred in bright spots with diameters of 1-10 microns and time durations in the 10-100 ps range. These time scales and dimensions are consistent with those expected for a magnetically driven collapse [11]. Our metric for a successful X-pinch target design is a load that produced a continuum x-ray source diameter  $<10$  microns over a time duration  $<1 \text{ ns}$ .

The x-ray pinhole camera on SATURN (described on page 29) has a spatial resolution of  $>200 \mu\text{m}$  at photon energies  $>2 \text{ keV}$  and a time gate of 3 ns, and is not sufficient to determine whether we were successful in producing a short-duration, small-diameter x-ray source. To make this measurement, we designed and built a slit-imaging camera following a technique similar to that employed previously [4,24]. The original camera resided on one of the three lines of sight (LOS C) on the SATURN facility. To improve the resolution of the instrument we later moved it inside the SATURN center section. This instrument is described on page 31. This instrument took several shot series to perfect, but we did succeed in getting useful data with it.

To measure the time duration of the  $>1$  keV x-ray emission, we relied on both photo-conducting diodes (PCDs) and an x-ray streak camera. The x-ray streak camera was installed before each shot series in which it was used, and then taken down again after the series was over. The limitation of the PCD time resolution was a sampling rate on the oscilloscope of 1 sample per 200 ps, which when coupled with the cabling probably limits the best time resolution to  $\sim 0.4$ - $0.5$  ns. The x-ray streak camera is in principle capable of significantly better time resolution, provided a relatively fast sweep rate is used. The x-ray streak camera diagnostic is described in detail on page 38. It proved to be somewhat difficult to field and reliably cross-time with SATURN, but did succeed in recording some data that showed features evolving on a shorter time scale than seen on PCDs.

The next level of sophistication beyond establishing that small-diameter, short-duration x-ray sources are present is to measure the plasma properties of such an x-ray source. This can be done with x-ray spectroscopy in the 1-10 keV range. The primary issue here is that in 0.2 MA experiments the line radiation persists for longer periods of time than the continuum radiation that comes from the smallest x-ray sources. In addition, the line radiation appears to come from a larger area. This appears to be because the line radiation is primarily emitted during or after the pinch has collapsed to a small radius, when the plasma is expanding again in size and/or beams are present. What this means in practice is that a time-resolved spectrometer is necessary to measure the changing plasma parameters, and that the conditions measured in a time-integrated spectrum are not necessarily representative of the plasma conditions in the small-diameter plasma. It also means that the time-resolved spectrum must have a time resolution comparable to the duration of the x-ray emission source, which means a time resolution  $<1$  ns, preferably more like 0.1 ns or better.

Our first goal was to create spectra that could be interpreted. For simplicity in analysis, we chose to focus on K-shell spectra from mid-Z ions (Cu, Ni, Mn). To this end, we began investigating alloys with these materials as the cross-points of solid X-pinch loads. To understand whether we were successful in creating the conditions needed to produce K-shell radiation, we fielded a time-integrated convex crystal spectrometer (see page 44).

Our ultimate goal was to field a streaked x-ray spectrometer using the same streak camera used for direct time duration measurements, with the idea that the streaked x-ray spectrometer would provide both a time duration measurement and a time-resolved spectrum. Unfortunately, this instrument proved too complex for us to successfully develop and field in the time frame of this project. It was fielded on two experiments, but there were design flaws that were not understood in time for any but the final experimental series on SATURN. The final experimental series used only pure tungsten targets, which were not conducive to spectroscopy and we opted to focus on getting direct streak data instead.

Thus, the project succeeded in making x-ray power and energy measurements, source size measurements, some time-duration measurements, and time-integrated spectroscopy measurements. The time duration measurements could have been improved to obtain better time resolution, and we failed to obtain any time-resolved spectroscopic measurements.



### 3. DESCRIPTION OF THE EXPERIMENTAL SETUP AND METHODS

#### 3.1 SATURN Power Feed Hardware

There were six experimental shot series on SATURN conducted as part of this research. Each series was assigned a different A-number for hardware drawing tracking and procurement purposes, as summarized in Table 1. The first set of experiments used SATURN in short-pulse mode, but with the large-diameter convolute most commonly used for long-pulse (~200 ns) experiments. It was suggested by the SATURN crew that subsequent experiments (also in short-pulse mode) switch to using the small-diameter convolutes, which was done. Cross-section views of the two different types of hardware are shown in Figure 3 and Figure 4.

A recurring problem throughout this research was that it was fairly difficult to set the vertical gaps for the radial power feed. The drawings for SATURN, including the MITL segments, do not exist electronically. The designers for the load hardware used old print drawings as their reference point for designing the load hardware, but some discrepancies exist between the resulting electronic drawings and the hardware presently in the chamber. We were not able to ascertain where the differences arose. As a result, the vertical gaps were manually adjusted by adjusting the MITL gaps directly, a sometimes time-consuming process.

The machine performance appeared to noticeably change in going from the large-diameter convolute to the small-diameter convolute, as measured by the load Bdots. The large-diameter hardware appeared to deliver higher currents to the load. We note, however, that the Bdots were located significantly farther out in this configuration, which may have made them less accurate for determining the current flowing through the cross-point, especially given the relatively long and narrow feed gap between the Bdot and the X-pinch target. Some evidence for this is found in the implosion times of the X-pinches. Despite the ostensibly higher currents during the first series, similar loads in series 2 had noticeably shorter implosion times.

**Table 1: Summary of hardware used during SATURN experiments**

Series	A Number	Shot Numbers	Description
1	A0014	3734-3737	High-number wire-array X-pinch scan
2	A0035 (sets 1-4)	3767, 3768, 3771	Nested wire-array X-pinch
2	A0035 (sets 5-6)	3769-3770	Tall solid X-pinch
3	A0047	3808-3814	Compact solid X-pinch
4	A0076	3857-3866	Compact solid X-pinch
5	A0110	3895-3900	Compact solid X-pinch
6	A0141	3940-3944	Compact solid X-pinch

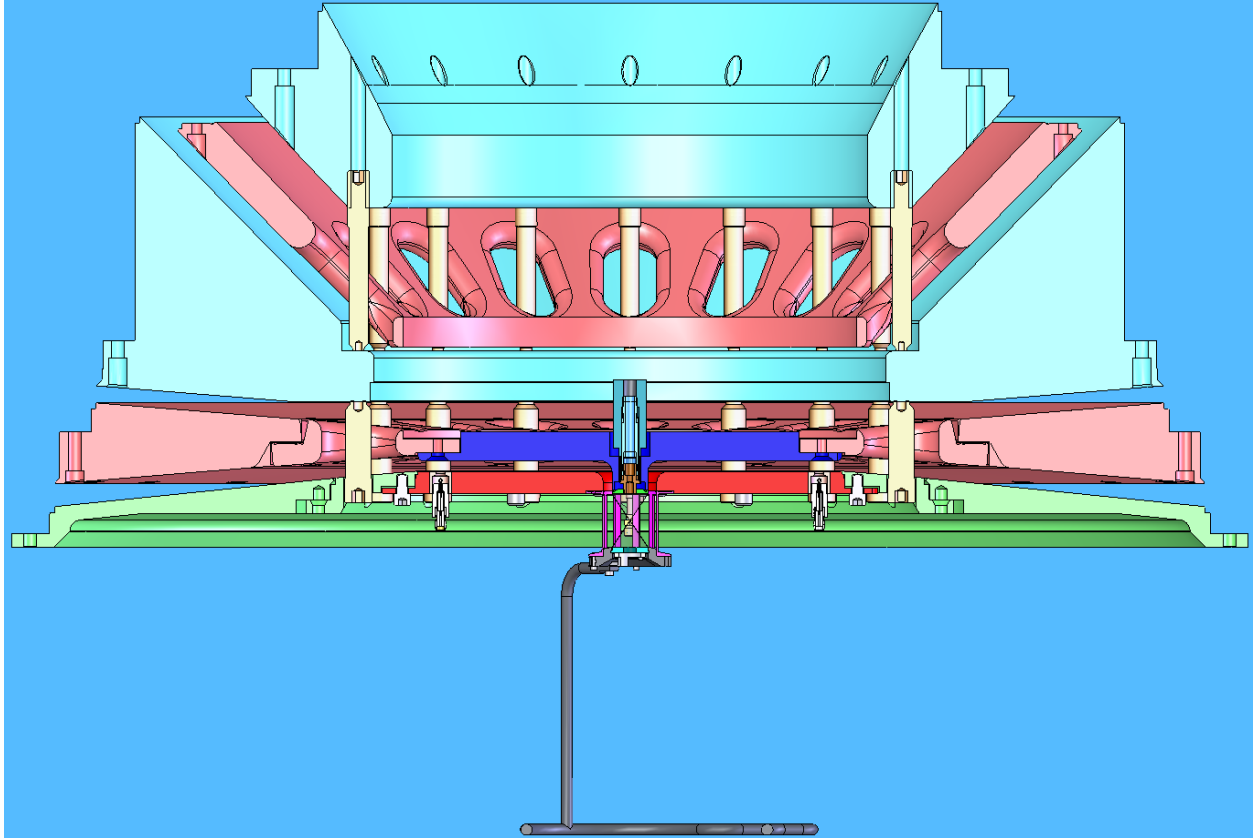


**Figure 3: Cross-section of wire-array X-pinch SATURN power feed hardware (A0019 only). Note that this hardware set used the large-diameter convolute.**

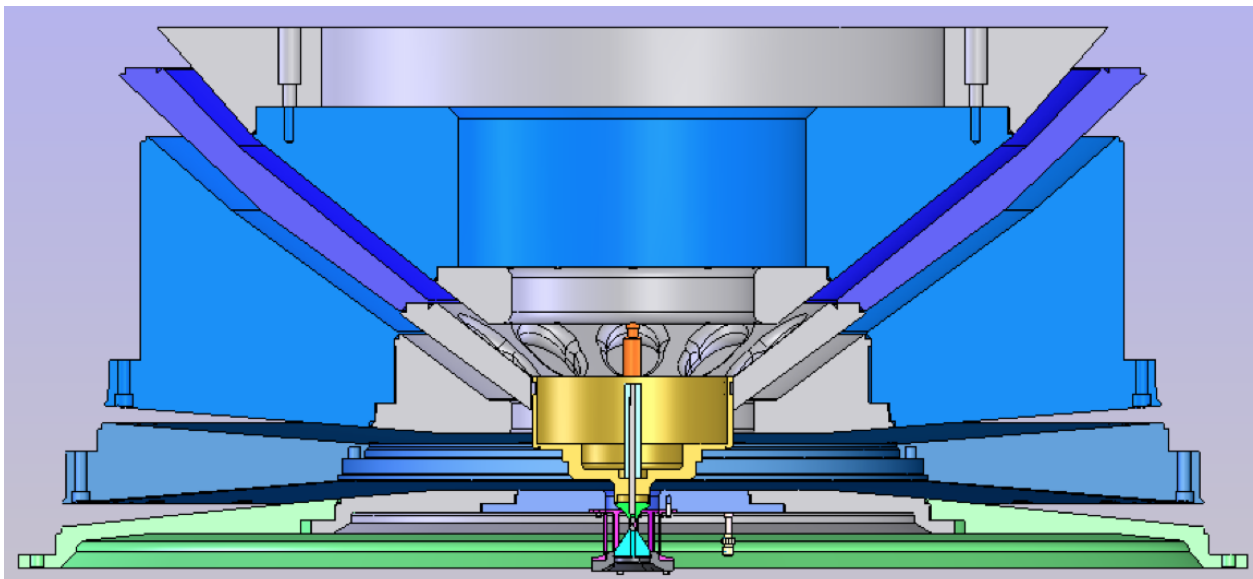


**Figure 4: Cross-Section of Solid X-pinch SATURN power feed hardware (A0035; A0047; A0076; A0110; A0141). Note that this hardware used the small-diameter convolute. The first four hardware sets in A0035 used a wire-array X-pinch target in place of the solid X-pinch hardware shown. The last two hardware sets in A0035 used a solid X-pinch target as shown, but the target X-pinch height in those targets matched the taller height of the wire-array X-pinch targets as discussed in Section 2.2**

### 3.2 X-pinch Target Hardware

The SATURN experiments used four basic types of targets: (i) high-number wire-array X pinches (Figure 5), (ii) nested wire-array X pinches (Figure 6), (iii) tall solid X pinches (Figure 7), and (iv) Compact solid X pinches (Figure 8). The high-number wire-array X pinches were used only during the first experimental series, when it was initially thought that a significantly larger mass/length would be required. The nested wire-array X pinches were only used during the second experimental series. The first design for the solid X pinch used targets designed to fit in the same return-current hardware as the wire-array X pinches from that series. After the second experimental series, which used the small-diameter convolute for the first time, there was interest in reducing the inductance of the load hardware to achieve a higher peak current. This was done by reducing the feed gap and also by reducing the total height of the X-pinch targets. Only the top (anode) half of the X-pinch could be reduced without affecting the diagnostic view of the cross-point. (The diagnostics all view the pinch from about 35-degrees below the horizontal, as illustrated in Figure 9). This led to the use of a more compact X-pinch target design, which was used for the remainder of the experimental campaigns.

A summary of the X-pinch target parameters used during the SATURN experiments can be found in Table 2. Several different elemental materials (Ti, Mo, W) and three alloys were used during the experiments. The composition of the three alloys is listed in Table 3. The alloy densities were not well known. An estimate of the alloy density was made using the individual elemental densities combined in a weighted average according to their atomic fractions. In the case of the nested wire array X-pinch targets, the density was estimated by calculating the total weight of the individual wires and using the estimated minimum radius based on the optimal wire packing geometry.

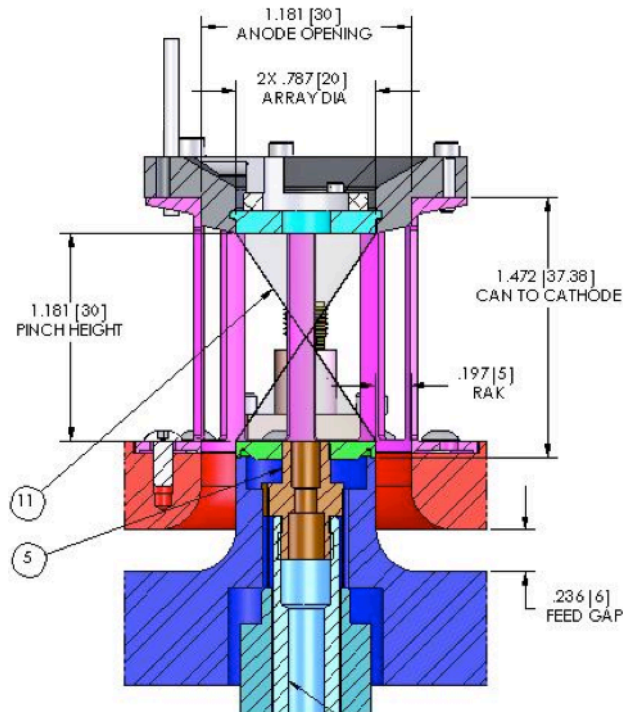


**Figure 5: Dimensions of the high-number wire-array X-pinch targets (A0019).**

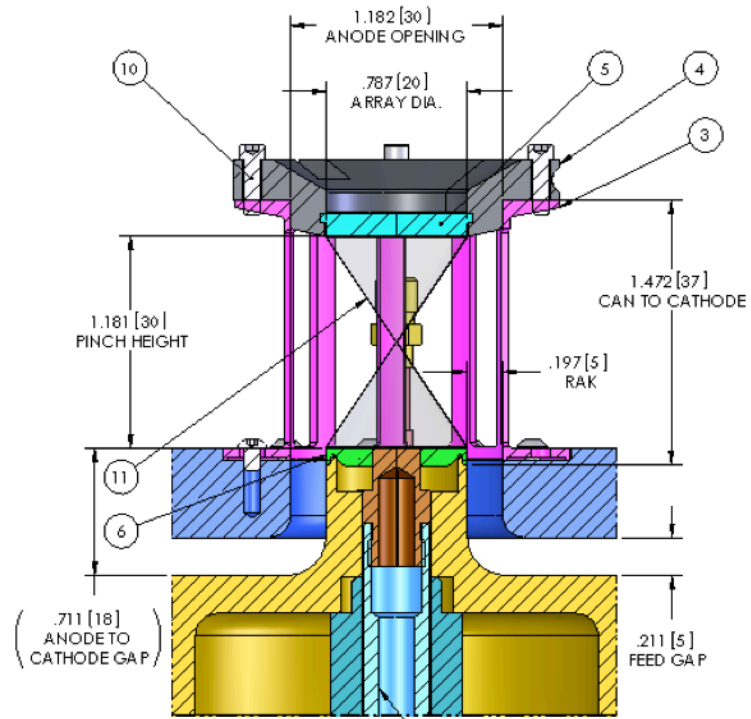


Figure 6: Dimensions of the nested wire-array X-pinch targets (A0035).

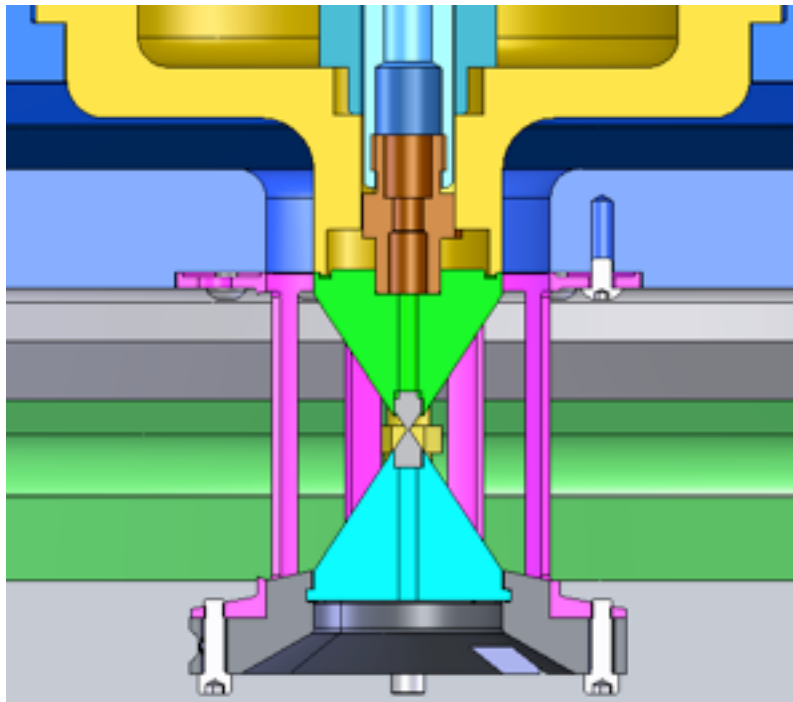
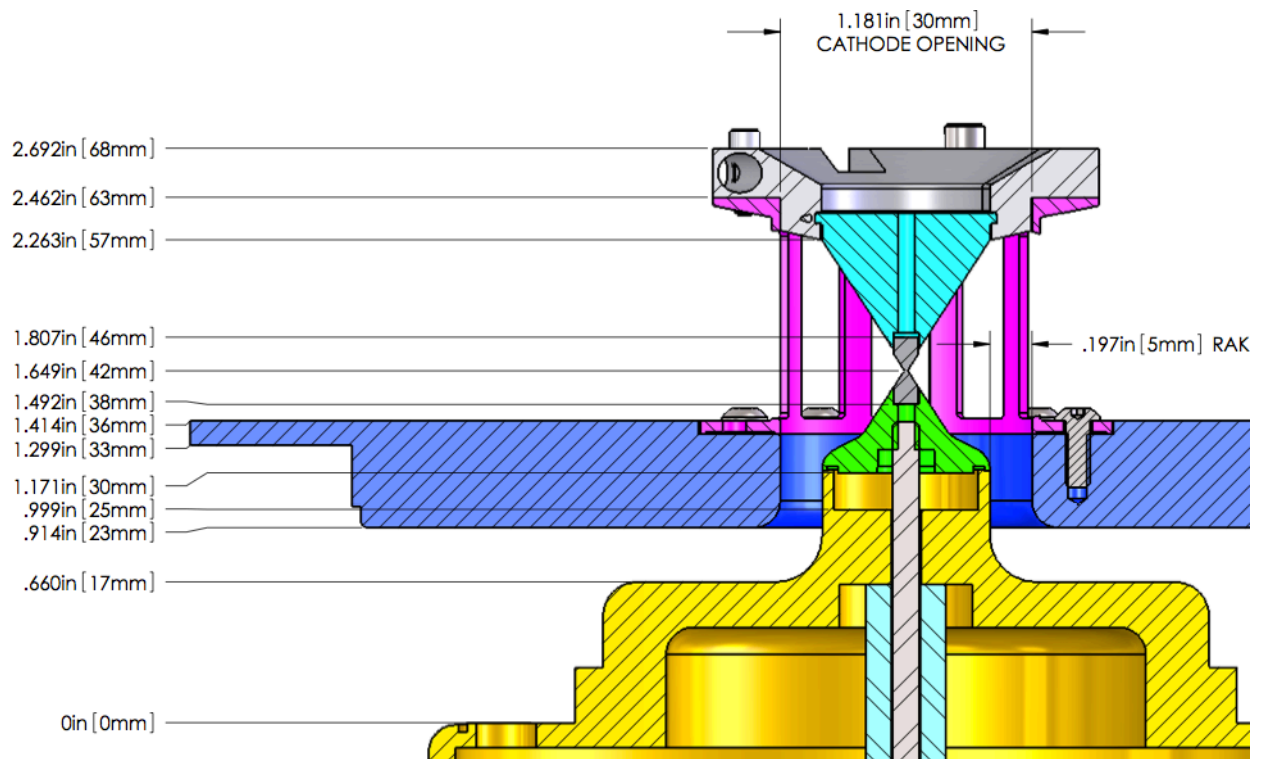
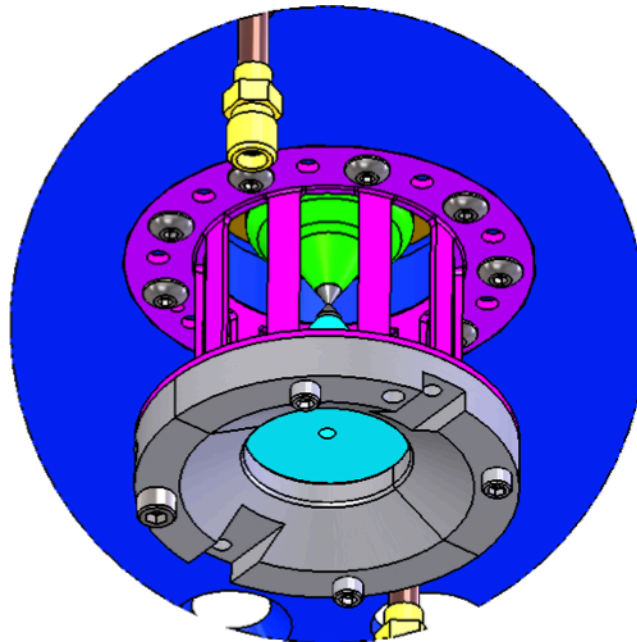


Figure 7: Drawing of the tall solid X-pinch targets (A0035). The target dimensions are identical to those of the nested wire-array X-pinch targets.



**Figure 8: Dimensions of the compact solid X-pinch targets (A0047, A0076, A0110, A0141).**



**Figure 9: Diagram illustrating the view of the X-pinch cross-point as seen from one of the LOS diagnostics. This extreme viewing angle constrained the load hardware design.**

**Table 2: Summary of the X-pinch target parameters on each shot**

Shot	Load	Mass/length (mg/cm)	Min. radius (microns)	Density (g/cc)
s3734	128x75 micron W	108	487.5	19.3
s3735	64x53 micron W	27	238.5	19.3
s3736	32x53 micron W	13.6	185.5	19.3
s3737	32x73 micron Mo	13.7	255.5	10.2
s3767	12x53 $\mu\text{m}$ W; 6x70.3 $\mu\text{m}$ W; 1x70.3 $\mu\text{m}$ W	13.2	158.5	19.3
s3768	12x70.3 $\mu\text{m}$ W; 6x83.3 $\mu\text{m}$ W; 1x83.3 $\mu\text{m}$ W	18.5	202.8	19.3
s3769	Solid W	14.1	152.5	19.3
s3770	Solid W	14.1	152.5	19.3
s3771	12x70.3 $\mu\text{m}$ W; 6x88 $\mu\text{m}$ Ti; 1x88 $\mu\text{m}$ Ti	12.8	202.3	
s3808	Solid Ni/Cr	11.6	209.8	8.4
s3809	Solid Cu/Ni	12	206.8	8.9
s3810	Solid W/Cu	15.2	183.4	14.4
s3811	Solid W/Cu	15.2	183.4	14.4
s3812	Solid Cu/Ni	12	206.8	8.9
s3813	prefire			
s3814	Solid Cu/Ni	12	206.8	8.9
s3857	Solid Cu/Ni	12	206.8	8.9
s3858	Solid Cu/Ni	12	206.8	8.9
s3859	Solid W/Cu	15.2	183.4	14.4
s3860	Solid W/Cu	15.2	183.4	14.4
s3865	Solid Cu/Ni	12	206.8	8.9
s3866	Solid Cu/Ni	12	206.8	8.9
s3895	Solid W (#1, 307 micron diam.)	14.1	153.5	19.3
s3896	Solid W/Cu (#2, 369 micron diam.)	15.2	184.5	14.4
s3897	Solid Cu/Ni (#2, 414 micron diam.)	12	207	8.9
s3898	Solid W (#4, 308 micron diam.)	14.1	154	19.3
s3899	Solid W/Cu (#4, 364 micron diam.)	15.2	182	14.4
s3900	Solid Ni/Cr	11.6	209.8	8.4
s3940	Solid W	20.3	183	19.3
s3941	Solid W	23.8	198	19.3
s3942	Solid W	23.8	198	19.3
s3944	Solid W	20.3	183	19.3

**Table 3: Summary of the properties of the Cu/Ni, W/Cu, and Ni/Cr alloys used.**

Material	wt %	amu	atomic frac.	atomic %
Cu	55	63.55	0.865	53.0
Ni	44	58.70	0.750	45.9
Mn	1	54.94	0.018	1.1
W	72	183.85	0.392	47.1
Cu	28	63.55	0.441	52.9
Ni	80	58.70	1.363	78.0
Cr	20	52.00	0.385	22.0

### 3.3 Diagnostic Description

#### 3.3.1 X-ray power and energy measurements

The x-ray power and energy yield was measured for the soft x-ray range (0.1-1 keV) using x-ray diodes (XRDs) [16,17] and nickel bolometers [18]. The x-ray power and energy yield for various hard x rays (>1 keV) was estimated using photoconducting diamond detectors (PCDs) [19,20] with various filters placed in front of them. These are standard power and energy diagnostics.

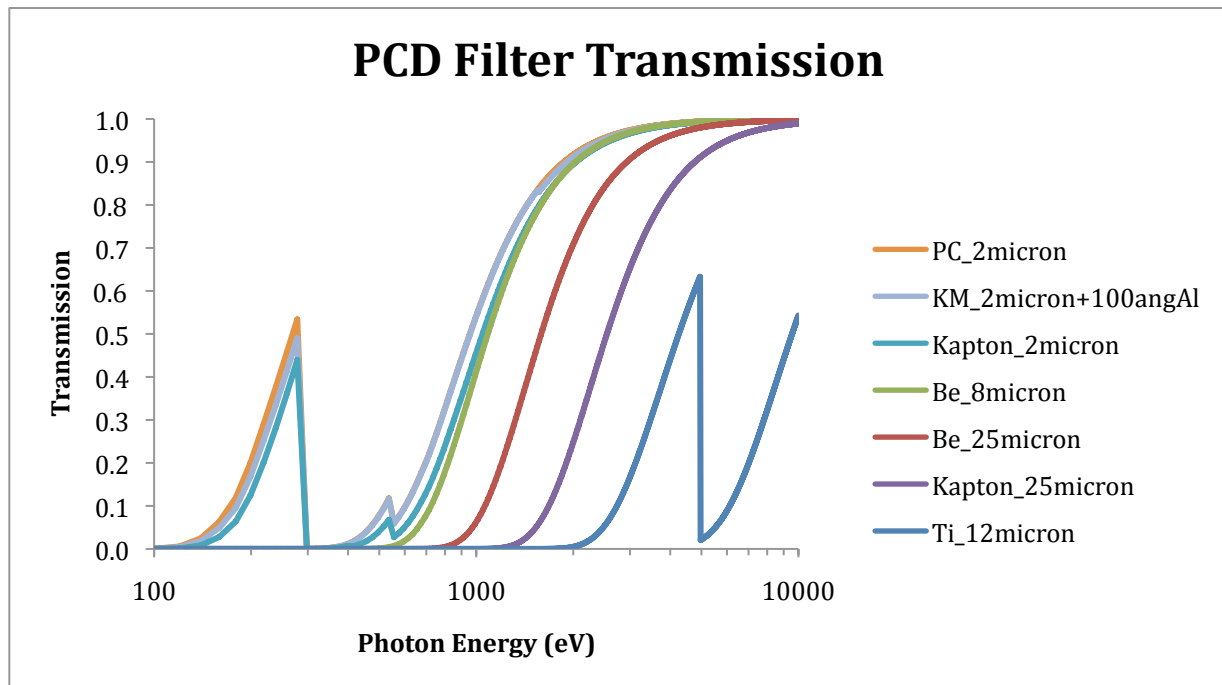


**Figure 10: Plot of PCD Filter Transmission vs. Photon Energy**

Due to availability and filter damage, the PCD elements used and their filter values changed several times during the six shot series on SATURN, which complicated some of the cross-comparisons. The PCD calibrations are estimated to be accurate to within +/-50%. The PCDs, XRDs, and bolometers were located a distance of 7.41 m from the load and viewed the load at an angle of about 35 degrees below the horizontal. On one experiment some XRDs were placed inside the vacuum chamber looking at the load nearly horizontally (0 degrees), and qualitatively the signals were identical, indicating that there were likely no significant shadowing effects. (The XRDs were destroyed by debris post-shot).

The remainder of this section contains a number of tables summarizing the configuration of these instruments, and Figure 11 contains some example radiation powers unfolded from the XRDs and PCDs.

**Table 4: List of PCD filters used on each shot.**

Shot	PCD #1	PCD #2	PCD #3	PCD #4	PCD #5
3734	25 $\mu$ m Kapton	2 $\mu$ m PC	12 $\mu$ m Ti	25 $\mu$ m Be	2 $\mu$ m KM
3735	25 $\mu$ m Kapton	2 $\mu$ m PC	12 $\mu$ m Ti	25 $\mu$ m Be	2 $\mu$ m KM
3736	25 $\mu$ m Kapton	2 $\mu$ m PC	12 $\mu$ m Ti	8 $\mu$ m Be	2 $\mu$ m KM
3737	25 $\mu$ m Kapton	2 $\mu$ m PC	12 $\mu$ m Ti	8 $\mu$ m Be	2 $\mu$ m KM
3767	25 $\mu$ m Kapton	2 $\mu$ m PC	12 $\mu$ m Ti	25 $\mu$ m Be	2 $\mu$ m KM
3768	25 $\mu$ m Kapton	2 $\mu$ m PC	12 $\mu$ m Ti	25 $\mu$ m Be	2 $\mu$ m KM
3769	25 $\mu$ m Kapton	2 $\mu$ m PC	12 $\mu$ m Ti	25 $\mu$ m Be	2 $\mu$ m KM
3770	25 $\mu$ m Kapton	2 $\mu$ m PC	12 $\mu$ m Ti	25 $\mu$ m Be	2 $\mu$ m KM
3771	25 $\mu$ m Kapton	2 $\mu$ m PC	12 $\mu$ m Ti	25 $\mu$ m Be	2 $\mu$ m KM
3808	25 $\mu$ m Kapton	2 $\mu$ m PC	12 $\mu$ m Ti	25 $\mu$ m Be	2 $\mu$ m KM
3809	25 $\mu$ m Kapton	2 $\mu$ m PC	12 $\mu$ m Ti	25 $\mu$ m Be	2 $\mu$ m KM
3810	25 $\mu$ m Kapton	2 $\mu$ m PC	12 $\mu$ m Ti	25 $\mu$ m Be	2 $\mu$ m KM
3811	25 $\mu$ m Kapton	2 $\mu$ m PC	12 $\mu$ m Ti	25 $\mu$ m Be	2 $\mu$ m KM
3812	25 $\mu$ m Kapton	2 $\mu$ m PC	12 $\mu$ m Ti	25 $\mu$ m Be	2 $\mu$ m KM
3814	25 $\mu$ m Kapton	2 $\mu$ m PC	12 $\mu$ m Ti	25 $\mu$ m Be	2 $\mu$ m KM
3857	25 $\mu$ m Kapton	2 $\mu$ m Kapton	12 $\mu$ m Ti	25 $\mu$ m Be	2 $\mu$ m KM
3858	25 $\mu$ m Kapton	2 $\mu$ m Kapton	12 $\mu$ m Ti	25 $\mu$ m Be	2 $\mu$ m KM
3859	25 $\mu$ m Kapton	2 $\mu$ m Kapton	12 $\mu$ m Ti	25 $\mu$ m Be	2 $\mu$ m KM
3860	25 $\mu$ m Kapton	2 $\mu$ m Kapton	12 $\mu$ m Ti	25 $\mu$ m Be	2 $\mu$ m KM
3865	25 $\mu$ m Kapton	2 $\mu$ m Kapton	12 $\mu$ m Ti	25 $\mu$ m Be	2 $\mu$ m KM
3866	25 $\mu$ m Kapton	2 $\mu$ m Kapton	12 $\mu$ m Ti	25 $\mu$ m Be	2 $\mu$ m KM
3895	25 $\mu$ m Kapton	2 $\mu$ m Kapton	12 $\mu$ m Ti	25 $\mu$ m Be	2 $\mu$ m KM
3896	25 $\mu$ m Kapton	2 $\mu$ m Kapton	12 $\mu$ m Ti	25 $\mu$ m Be	2 $\mu$ m KM
3897	25 $\mu$ m Kapton	2 $\mu$ m Kapton	12 $\mu$ m Ti	25 $\mu$ m Be	2 $\mu$ m KM
3898	25 $\mu$ m Kapton	2 $\mu$ m Kapton	12 $\mu$ m Ti	25 $\mu$ m Be	2 $\mu$ m KM
3899	25 $\mu$ m Kapton	2 $\mu$ m Kapton	12 $\mu$ m Ti	25 $\mu$ m Be	2 $\mu$ m KM
3900	25 $\mu$ m Kapton	2 $\mu$ m Kapton	12 $\mu$ m Ti	25 $\mu$ m Be	2 $\mu$ m KM
3940	25 $\mu$ m Kapton	2 $\mu$ m Kapton	12 $\mu$ m Ti	25 $\mu$ m Be	2 $\mu$ m KM
3941	25 $\mu$ m Kapton	2 $\mu$ m Kapton	12 $\mu$ m Ti	25 $\mu$ m Be	2 $\mu$ m KM
3942	25 $\mu$ m Kapton	2 $\mu$ m Kapton	12 $\mu$ m Ti	25 $\mu$ m Be	2 $\mu$ m KM
3944	25 $\mu$ m Kapton	2 $\mu$ m Kapton	12 $\mu$ m Ti	25 $\mu$ m Be	2 $\mu$ m KM

**Table 5: List of selected PCD peak powers and radiated energy by shot.**

Shot	12 micron Ti Peak Power (GW)	12 micron Ti Net Energy (J)	25 micron Be Peak Power (GW)	25 micron Be Net Energy (J)
3734	21	122	NA	NA
3735	>63.8*	>885.1*	34	19
3736	255	1631	NA	NA
3737	127	1014	NA	NA
3767	NA	NA	NA	NA
3768	7.6?	25.6?	>93.1*	>1312.2*
3769	70	221	>186.5*	>2732.6*
3770	22	163	424	3672
3771	49	235	576	5304
3808	12	79	129	1325
3809	13	79	216	1843
3810	64	283	>255.8*	>3831.2*
3811	62	151	497	3458
3812	16	51	203	1560
3814	14	59	259	1188
3857	3	33	44	354
3858	19	127	194	1797
3859	89	210	481	3508
3860	15	88	186	1842
3865	15	99	229	1412
3866	14	44	257	996
3895	NA	NA	56	173
3896	41	148	407	3916
3897	26	113	124	1137
3898	NA	NA	NA	NA
3899	29	107	301	2708
3900	36	122	246	1593
3940	53	152	400	2415
3941	84	356	495	5188
3942	21	92	304	1906
3944	43	127	219	1965

\* = Signal data peak clipped on oscilloscope

NA = Data not available for this shot

**Table 6: Bolometer radiation energy and peak power by shot.**

Shot	101 Energy (kJ)	113 Energy (kJ)	Avg. Energy (kJ)	101 Power (TW)	113 Power (TW)	Avg. Power (TW)	Notes
3734	56	91	73	3.4	5.6	4.5	Old bolo current pulser
3735	166	224	195	7.3	9.8	8.6	Old bolo current pulser
3736	147	193	170	5.3	7.0	6.2	Old bolo current pulser
3737	148	189	168	4.3	5.5	4.9	Old bolo current pulser
3767	125	137	131	5.1	5.6	5.4	Old bolo current pulser
3768	89	96	92	3.4	3.8	3.6	Old bolo current pulser
3769	118	140	129	11.6	13.8	12.7	Old bolo current pulser
3770	87	98	92	5.3	5.9	5.6	Old bolo current pulser
3771	115	135	125	5.8	6.9	6.4	Old bolo current pulser
3808	168	143	156	13.1	11.2	12.2	x2?
3809	96	83	90	5.9	5.0	5.5	
3810	173	152	162	13.6	11.9	12.8	
3811	194	164	179	10.6	9.0	9.8	
3812	153	117	135	5.7	4.3	5.0	
3814	78	61	70	8.4	6.6	7.5	
3857	119	122	121	4.2	4.2	4.2	
3858	126	130	128	8.0	8.1	8.1	
3859	160	169	165	9.1	9.7	9.4	
3860	144	151	147	10.2	10.7	10.5	
3865	97	100	99	7.6	7.9	7.8	
3866	109	117	113	10.6	11.3	11.0	
3895	56	64	60	3.1	3.6	3.4	
3896	224	270	247	10.5	12.6	11.6	
3897	117	139	128	11.0	12.9	12.0	
3898	18	23	20	0.6	0.7	0.7	
3899	136	166	151	7.9	9.6	8.8	
3900	109	128	119	9.4	11.0	10.2	
3940	133	154	144	8.9	10.3	9.6	
3941	172	203	187	8.4	9.9	9.2	
3942	102	120	111	8.0	9.5	8.8	
3944	117	132	124	8.2	9.3	8.8	

**Table 7: List of implosion parameters by shot and type. For the purposes of estimating the implosion time, the start time was defined as  $t_0 = t(2.8 \text{ MA}) - 50 \text{ ns}$  (except s3898).**

Shot	Load	Timp* (ns)	Imax (MA)	PI
s3734	128x75 micron W	120,154,176	5.9	7
s3735	64x53 micron W	78, <b>88</b> ,98	4.9	111
s3736	32x53 micron W	<b>82</b>	6.2	364
s3737	32x73 micron Mo	<b>89</b> ,102	6.9	190
s3767	12x53 $\mu\text{m}$ W; 6x70.3 $\mu\text{m}$ W; 1x70.3 $\mu\text{m}$ W	64,75	4.3	513
s3768	12x70.3 $\mu\text{m}$ W; 6x83.3 $\mu\text{m}$ W; 1x83.3 $\mu\text{m}$ W	<b>65</b>	3.7	224
s3769	Solid W	<b>62</b> ,69	5.8	519
s3770	Solid W	<b>51</b> ,77	5.5	519
s3771	12x70.3 $\mu\text{m}$ W; 6x88 $\mu\text{m}$ Ti; 1x88 $\mu\text{m}$ Ti	48,64, <b>68</b>	4.7	325
s3808	Solid Ni/Cr	<b>72</b>	5.6	333
s3809	Solid Cu/Ni	60, <b>64</b> ,69	5.8	332
s3810	Solid W/Cu	<b>62</b>	5.5	333
s3811	Solid W/Cu	<b>69</b> ,78	5.9	333
s3812	Solid Cu/Ni	<b>62</b>	6.0	332
s3813	prefire	--	--	--
s3814	Solid Cu/Ni	<b>63</b>	5.8	332
s3857	Solid Cu/Ni	56,61,65,70,92	5.5	332
s3858	Solid Cu/Ni	69, <b>67</b>	5.9	332
s3859	Solid W/Cu	45,53, <b>62</b>	5.9	333
s3860	Solid W/Cu	<b>53</b> ,63	5.3	333
s3865	Solid Cu/Ni	55, <b>59</b>	5.6	332
s3866	Solid Cu/Ni	<b>65</b>	5.7	332
s3895	Solid W (#1, 307 micron diam.)	<b>46</b>	4.7	512
s3896	Solid W/Cu (#2, 369 micron diam.)	<b>68</b> ,72	5.6	329
s3897	Solid Cu/Ni (#2, 414 micron diam.)	<b>53</b> ,58	5.4	331
s3898	Solid W (#4, 308 micron diam.)	52,65	2.8	509
s3899	Solid W/Cu (#4, 364 micron diam.)	<b>44</b> ,64, <b>72</b>	5.8	338
s3900	Solid Ni/Cr	<b>54</b> ,67	5.9	333
s3940	Solid W	<b>50</b>	5.8	250
s3941	Solid W	52, <b>56</b>	5.8	182
s3942	Solid W	46,56, <b>62</b> ,64	5.8	182
s3944	Solid W	55, <b>57</b> ,61,66	5.7	250

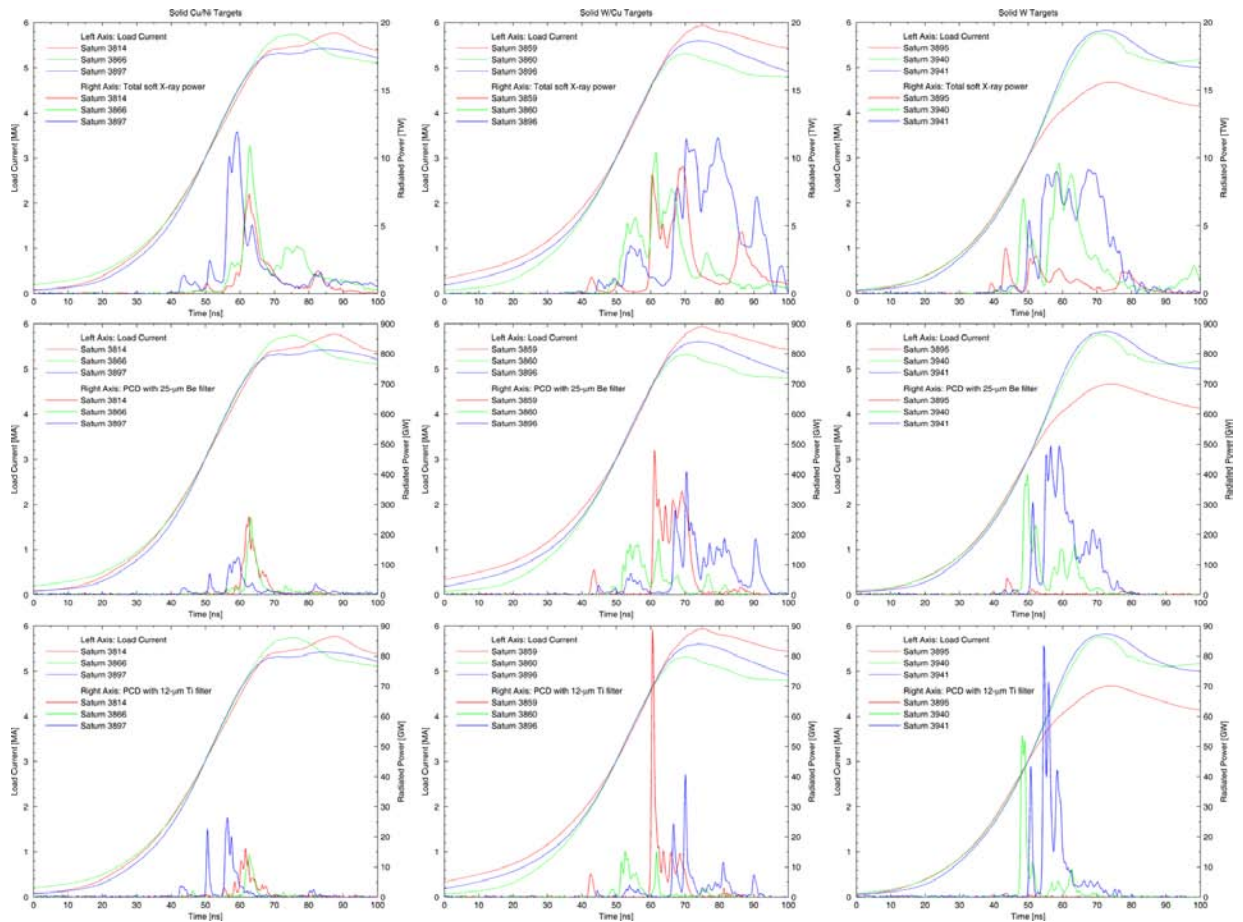


**Figure 11: Example radiation powers for selected X-pinch tests. The columns show data from solid Cu/Ni, W/Cu, and W X-pinch loads, respectively. The rows show the total soft ( $\sim 0.1\text{-}1$  keV) x-ray power, the  $>1$  keV x-ray power, and the 3-5 keV x-ray power, respectively. Based on the MLM images, the total power is believed to come from a height of  $\sim 3$  mm.**

### 3.3.2 X-ray imaging measurements

Traditional x-ray pinhole cameras fundamentally consist of an x-ray source, a pinhole imaging aperture, and a detector. The spectral range of the pinhole is usually selected through the use of a filter material, and the filters are usually chosen to have an edge somewhere in the 0.1-1 keV range. Nearly all filters eventually become nearly 100% transmissive at higher photon energies as seen in Figure 10. Thus, a filter chosen to pass ~300-500 eV x rays might also have near 100% transmission for x rays >2000 eV. This makes the resulting image a composite of both soft x rays and hard x rays, making the true spectral composition of the image ambiguous.

To obtain near-monochromatic x-ray imaging <1000 eV, the traditional pinhole imaging system can be modified to insert a flat multi-layer mirror. The mirror bi-layer period and angle can be chosen so that only x rays satisfying the Bragg condition are diffracted (reflected) from the surface of the mirror. Such a pinhole camera system was designed for SATURN [21,22,23] that obtains <10 eV bandwidth at a photon energy of 277 eV using a Cr/C multilayer mirror with a grazing angle of about 34 degrees. The images are time-gated with 1 ns time resolution.

This diagnostic is useful for measuring the spatial structure of the low- and high-energy x-ray emission. Its main limitation for this project is that it has relatively poor spatial resolution. The spatial resolution of a pinhole imaging system is limited by both diffraction from the pinhole itself, which worsens the resolution as the pinhole diameter shrinks, and by the pinhole imaging optical geometry, which worsens the resolution as the pinhole diameter increases. For 277 eV, the optimal pinhole diameter that maximizes the spatial resolution gives a spatial resolution of 482 microns. This is large compared to the spatial extent of the cross point region of the X pinch.

The SATURN MLM diagnostic is shown in Figure 12, and is a permanent facility diagnostic. Example data from the MLM instrument obtained during this project is shown in Figure 13. The hard x-ray channel used 8 microns of Be + 1 micron CH, which transmits broadband radiation >1 keV. For the dimensions used in the MLM the spatial resolution for the hard x-ray channel is about 200 microns. As the figure indicates, the x-ray source size in hard radiation is smaller than in soft radiation. An approximate upper bound for the soft x-ray radiation of about 3 mm is obtained from this analysis, though the source clearly has significant structure during this time. The hard x-ray images also clearly show that the first several bursts of hard x rays seen on the PCDs are initially from very small x-ray source sizes. The late-time radiation comes from a larger area and is presumed to be the result of the pinch breaking up and possibly creating beams in the resulting gap, as is the case in 200 kA X-pinch data.

During the first SATURN experiments we obtained time-integrated >1 keV x-ray images using a hard x-ray pinhole camera. It was extremely cumbersome to use and didn't have particularly good spatial resolution, however, so it was dropped in subsequent series. Similarly, a time-resolved "quad camera" was loaned to the project by Imperial College for the first shots, but was unavailable for subsequent shots. The few results from these diagnostics are consistent with the results from the MLM camera shown here.

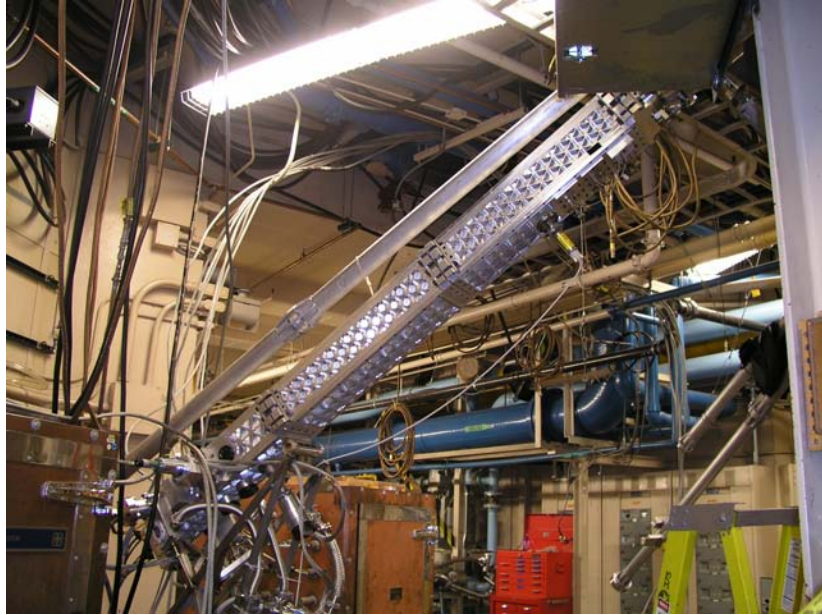


Figure 12: Photo of LOS B. The MLM instrument is the square cross-section piece with the honeycomb structure. The XRDs were located on the pipe above the MLM.

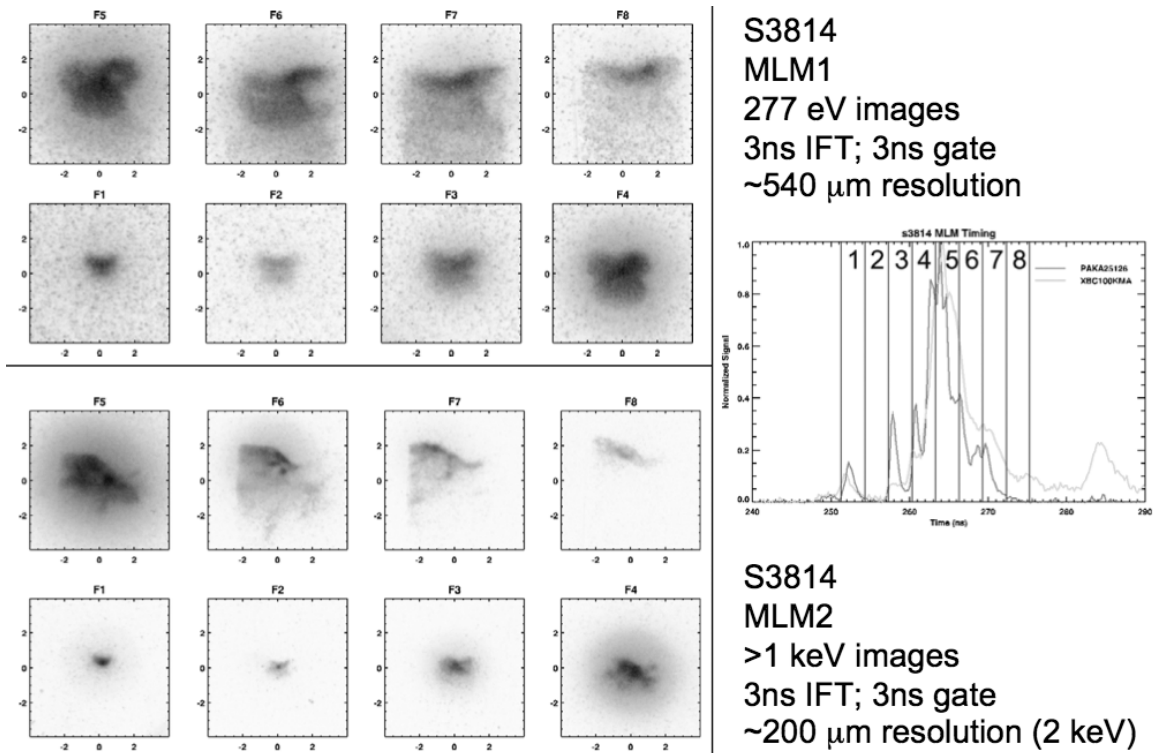
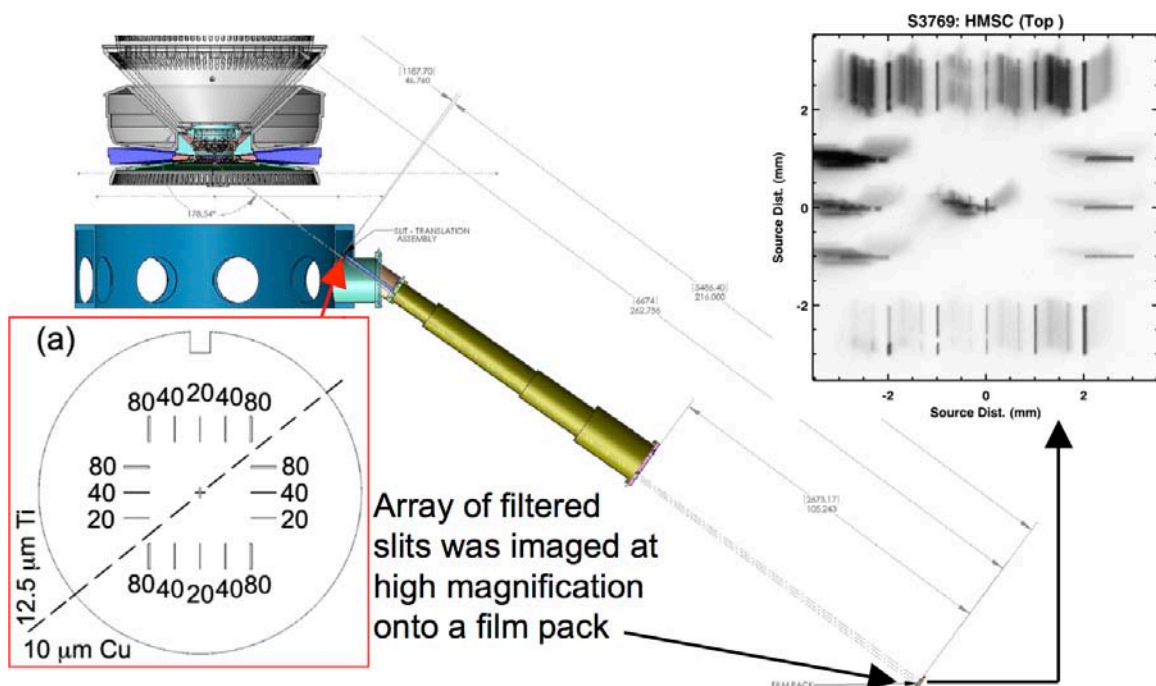


Figure 13: Example MLM data from s3814 (solid Cu/Ni X pinch)

### 3.3.3 X-ray spot size measurements

Previous work on 200 kA Mo X pinches measured the time-integrated x-ray source size in the 3–5 keV range using slits of different sizes from 1 to 50  $\mu\text{m}$  in width [4]. The idea is that an x-ray source size with dimension smaller than this would create a point-projection radiograph image of the slit. Though they fabricated slits that were very small, due to the very weak signals from the smaller slits the majority of the analysis in those experiments was done using a 40  $\mu\text{m}$  slit. In those experiments, the slits were 13.7 cm from the source and the detector was 92.7 cm from the source, for a magnification of 6.77. They inferred that in some experiments Mo X pinches at 200 kA could produce  $1.2 \pm 0.5 \mu\text{m}$  x-ray spots in 2.8–5 keV emission [4].

We performed a similar measurement during these experiments using a similar technique to that employed on previous 1 MA X-pinch experiments at Cornell [24]. An array composed of several 20-, 40-, and 80- $\mu\text{m}$  wide vertical and horizontal slits was made in a 25- $\mu\text{m}$  thick Ta foil, as shown in Figure 14. During the first two experimental shot series (s3734-s3737 and s3767-s3771) the slit was located a distance of 1.187 m from the target and the detector (x-ray film) was located 6.674 m away on LOS C, for a magnification of 5.62. By measuring the sharpness of the slit image edge, it is possible to estimate the size of the source. For such a long distance, however, Fresnel diffraction effects limit the minimum observable slit edge width to roughly  $\delta \sim \sqrt{\lambda d}$ , which for  $\lambda \sim 3.6$  Angstroms (3.5 keV) and a slit distance  $d$  of 1.1 m corresponds to about 20  $\mu\text{m}$ . To accurately measure sources smaller than this requires a slit closer to the load.



**Figure 14: Schematic diagram of slit camera designed for the first SATURN shot series (s3734-3737). The design was abandoned because x-ray diffraction was limiting the source size determination to  $\sim 20$  microns.**

Subsequent tests used a custom-built slit-imaging camera inside the SATURN vacuum chamber, shown in Figure 15 and Figure 16. In this geometry the slit was located 0.1 m from the load and

the detector was 0.66 m from the load, for a magnification of 6.6. Fresnel diffraction in this case limits the slit width to more like 6 microns, making it easier to resolve very small sources. Unfortunately, the x-ray background inside the chamber was extremely large and we lost most of the data from series 3 (s3808-s3814) while optimizing the new instrument. Ultimately we were required to use much thicker in-line baffling in addition to the 25- $\mu\text{m}$  thick Ta foil in which the slits were cut to reduce the background signals from high-energy bremsstrahlung being created near the load. As a result, the slit images obtained with this instrument were always superimposed upon a significant background.

To select the spectral range used to create the slit images, we placed two filters in front of the slit array, each covering half of the slits along a diagonal axis of symmetry. The filter materials were always Ti and Cu, but the filter thicknesses and films used varied as shown in Table 8. These filters, when used with Mo or W X-pinch sources, do not transmit any strong thermal line emission, which has been shown in 200 kA experiments to come from a large region, not just the bright spot [5]. Characteristic W L-shell radiation usually gives smooth, wide images that are easily distinguished from hot-spot radiation.

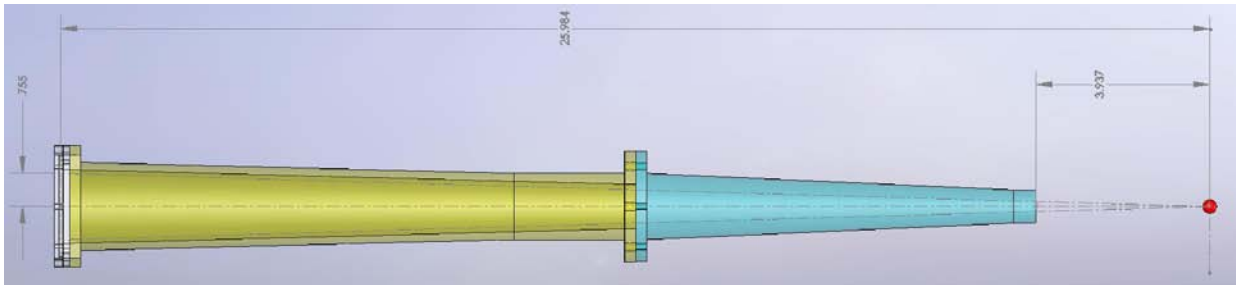


**Figure 15: Cross-section of the in-chamber high-magnification slit camera used to measure the x-ray spot size.**



**Figure 16: Photo of SATURN center section showing the slit camera (to the left of the author) and the time-integrated convex crystal spectrometer (above author).**

**Table 8: Filter and film configuration for the high-magnification slit camera (HMSC). The Cu and Ti filters were each applied to only half of the slits as shown in Figure 14(a). The Kapton filters were applied to the entire image. All filter thicknesses are in microns. The Cu-filtered slits were always up in the real world. The films are all from Kodak.**

Shot(s)	Cu	Ti	Kapton	Between 2nd/3rd film	Films
s3734-s3737	10	12.5	100	n/a	3x TMAX-400
s3767-s3771	10	12.5	100	n/a	3x TMAX-400
s3808-s3814	60	87.5	100	n/a	3x TMAX-400
s3857-s3858	60	87.5	150	n/a	3x TMAX-400
s3859	60	87.5	150	n/a	2x TMAX-100 + 1x TMAX-400
s3860-s3865	40	50	150	n/a	2x TMAX-100 + 1x TMAX-400
s3866	40	50	150	n/a	2x TMAX-100 + 1x DR-50
s3895-s3899	40	50	150	100 Kapton	2x TMAX-100 + 1x DR-50
s3900	40	50	100	100 Kapton	2x TMAX-100 + 1x DR-50
s3940-s3942	40	50	150	100 Kapton	2x TMAX-100 + 1x DR-50
s3943	40	50	150	n/a	2x TMAX-100 + 1x DR-50

The varying filter and film combination used in the high-magnification slit camera (HMSC) during the course of this project are summarized in Table 8. The transmission through each of these filters is shown in Figure 17. Much of our best data was obtained in the later shot series, and the net filtration for the first film is shown in Figure 18. Note that the bottom films in the film stack would be filtered slightly more than this by any films above it. Each film's filtration can be quickly estimated as an extra ~150 microns of Kapton.

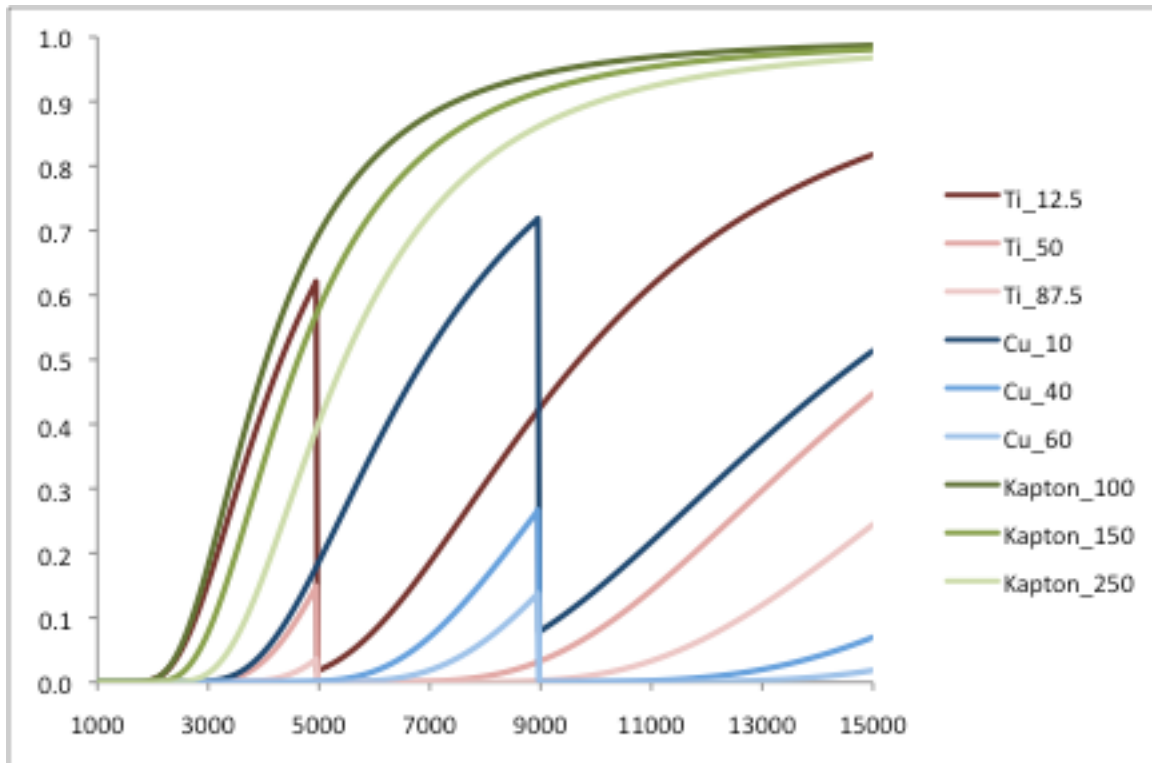


**Figure 17: Plot of HMSC filter transmissions versus photon energy for all filters used during the course of this project.**

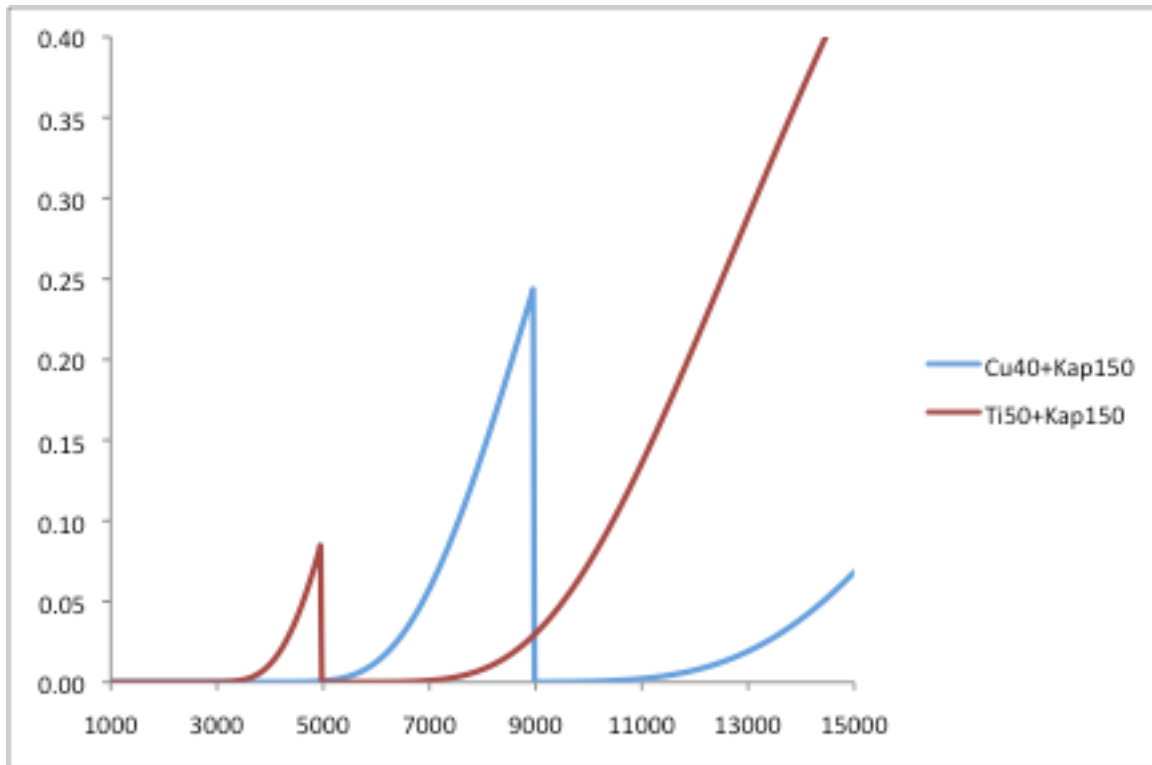


**Figure 18: Plot of HMSC filter transmission vs. photon energy for one of the most common configurations for which data was obtained.**

We note that while it may appear that the images created by the filters shown in Figure 18 might be dominated by  $>9$  keV radiation, we do not believe this to be the case. The radiation is expected to be essentially blackbody radiation due to the high densities and temperatures believed to exist in the micropinch plasma. The intensity of the brightest spots seen in the x-ray streak camera film suggest that the radiation  $>2.5$  keV may be roughly 50% of the radiation  $>1.5$  keV. This would be consistent with a  $\sim 600$  eV blackbody (very approximate). The radiation intensity at 9 keV from a 600 eV blackbody is  $\sim 135$ x less than the radiation intensity at 5 keV, so the contribution to the images from radiation  $>9$  keV is expected to be negligible.

The remainder of this section shows example data from s3769 in Figure 19 and from s3941 in Figure 20 and Figure 21. These data show that at least some SATURN X pinches were capable of producing x-ray bursts with a source diameter of 5-7 microns.

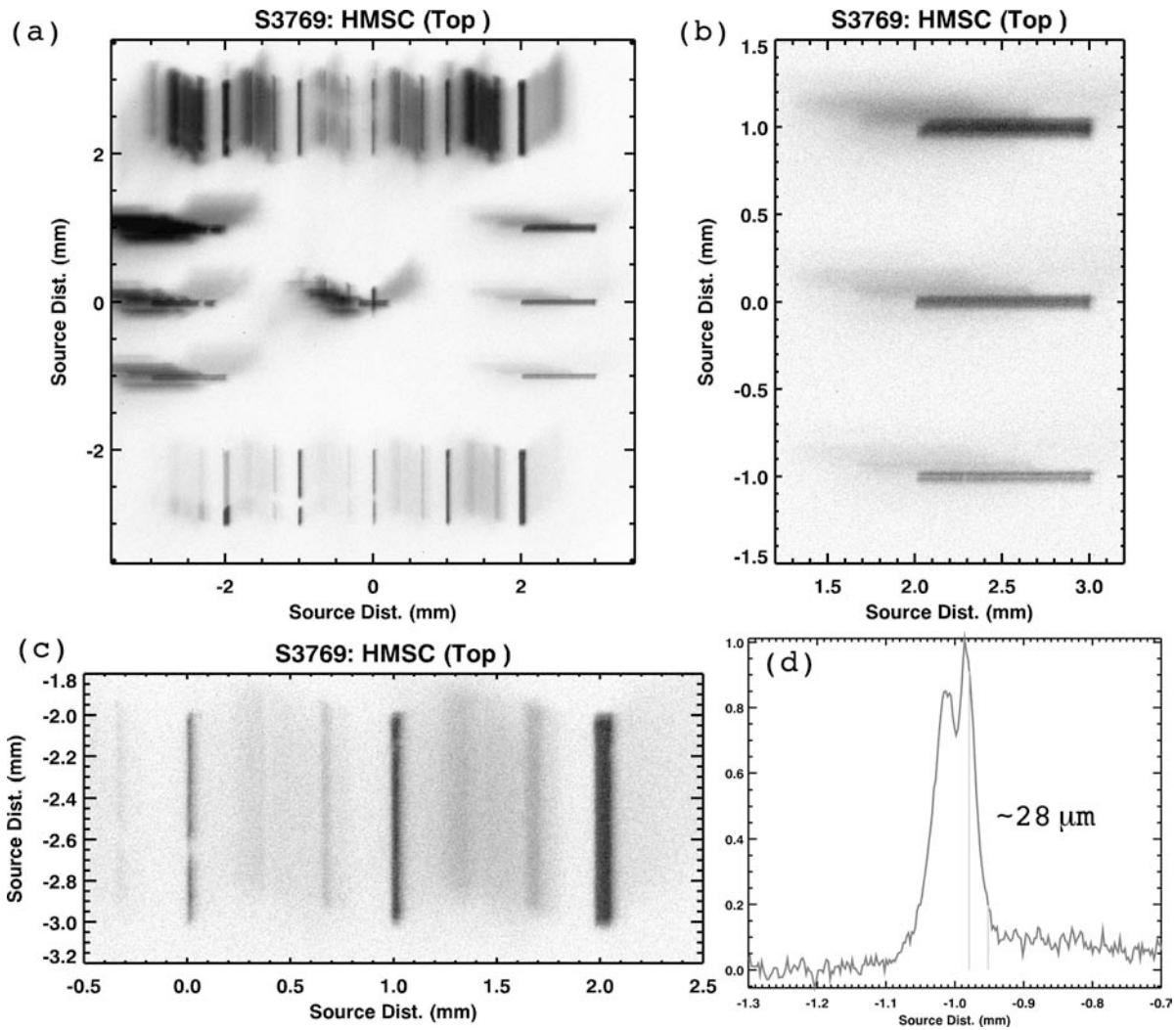


**Figure 19: Example high-magnification slit camera data (LOS version) from s3769, a solid tungsten X-pinch load. The entire film is shown in (a), along with expanded views of the Cu-filtered (b) horizontal and (c) vertical slits. Looking carefully at the two sets of slit images, one can see that two relatively small x-ray sources were produced, displaced mainly vertically from one another. From the data we can determine that the sources were separated by 32 microns along the vertical direction. A lineout through the 20-micron slit data is shown in (d), in which it can be seen that the edge is approximately 28 microns wide. Much of this may be due to diffraction effects, which is estimated to blur a sharp edge to  $\sim 21$  microns at the distances used in this diagnostic.**

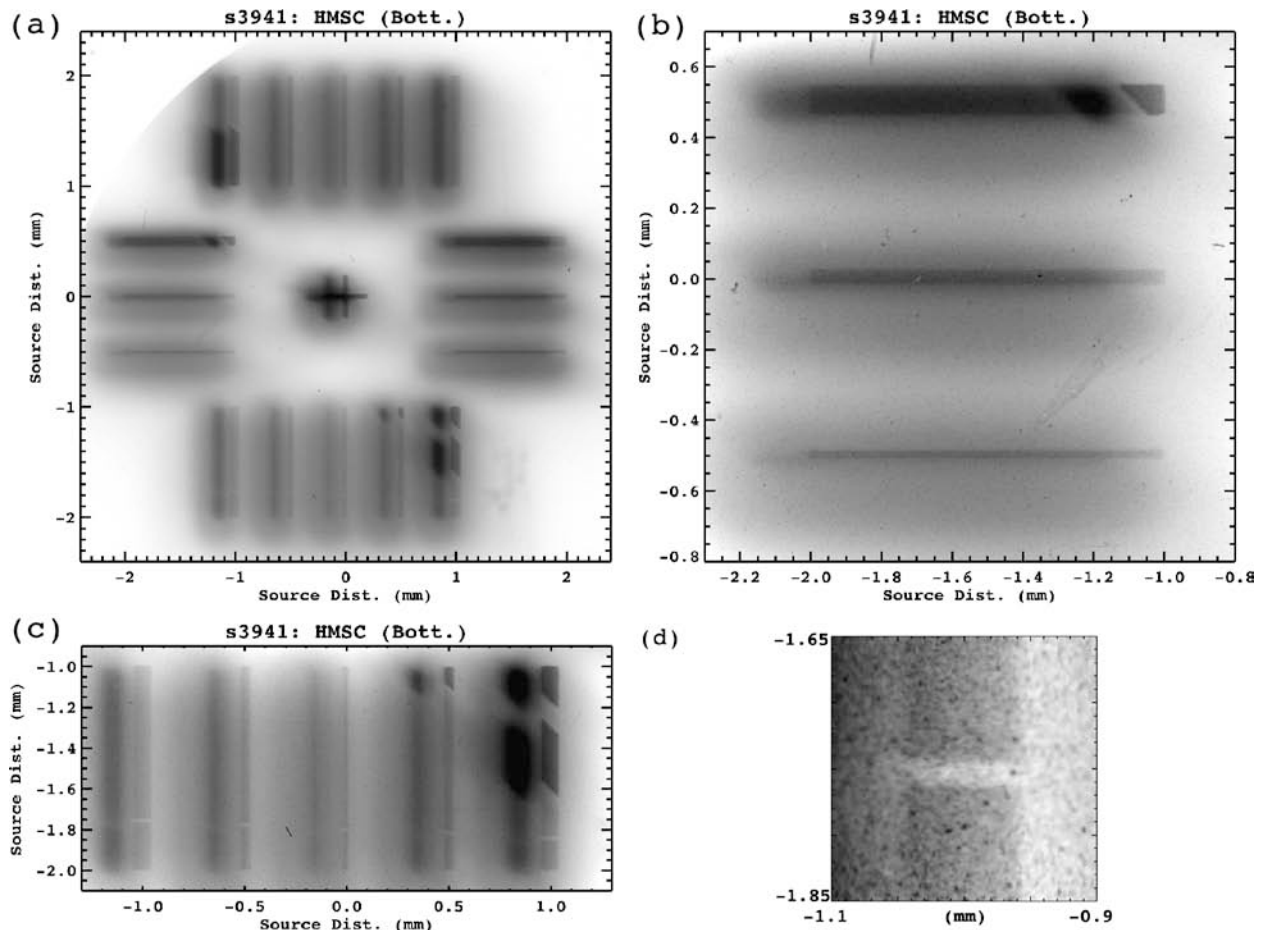


**Figure 20: Example high-magnification slit camera data (center section version) from s3941, a solid tungsten X-pinch load. The entire film is shown in (a), along with expanded views of the Cu-filtered (b) horizontal and (c) vertical slits. In this case one small-diameter source was produced and a second, more intense but larger-size source was also produced that was shifted about 177 microns horizontally. The diagonal variations in the intensity from the upper left to the lower right are caused by imperfect slit filter alignments. On this test an 18.5-micron diameter stainless steel wire was strung across the bottom slits, as shown in an expanded view in (d).**

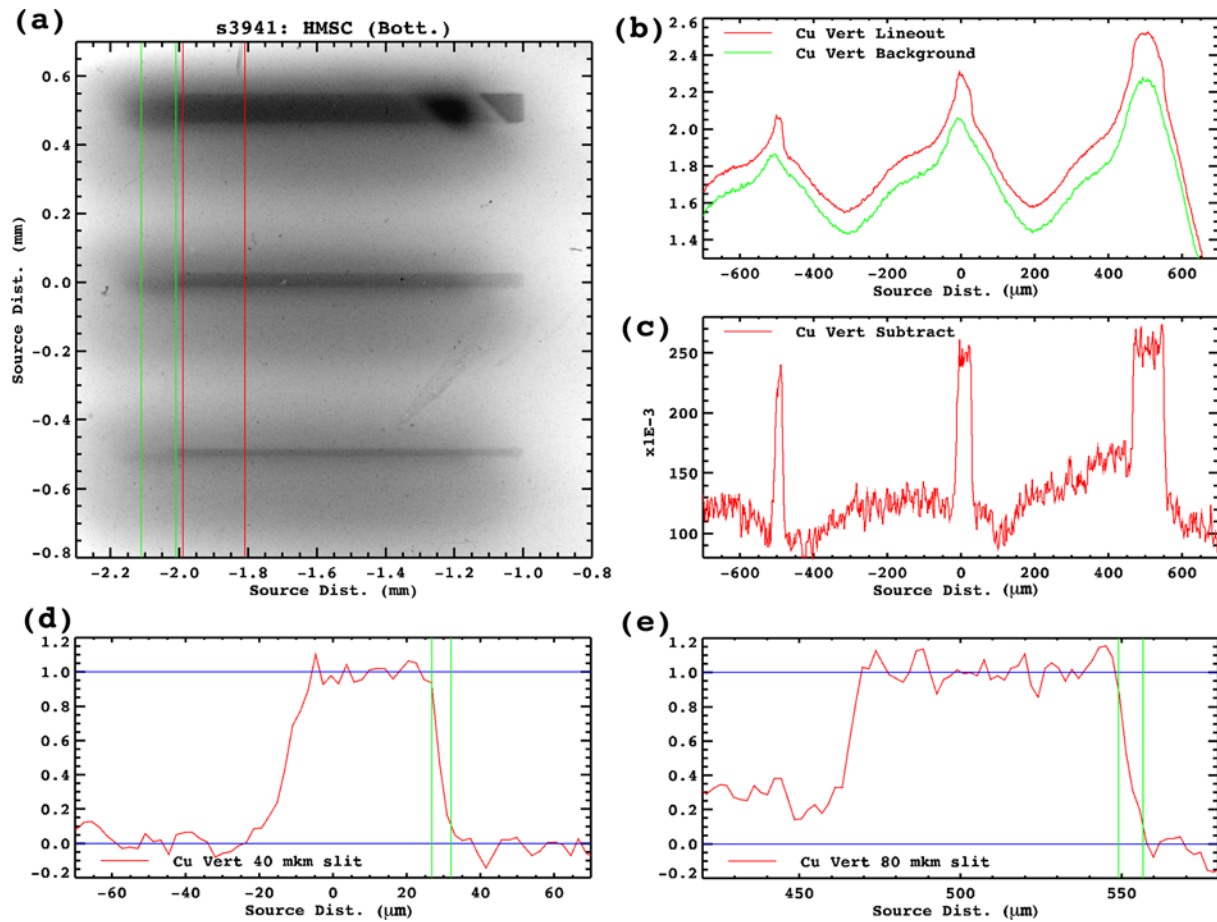


**Figure 21: Lineouts through the Cu-filtered slit data from s3941, a solid tungsten X-pinch load. The second, larger-diameter source made it difficult to extract the sharper image. Two lineouts through the image were made, shown in part (a), and are plotted in (b). The lineouts were subtracted to produce the plot shown in (c). The 10-90% edge distances are measured in parts (d) and (e), and are 5.2 and 7.6 microns, respectively.**

### 3.3.4 X-ray streak camera measurements

Past x-ray streak camera measurements with 200 kA Mo X pinches demonstrated x-ray bursts in the 10–100 ps time range [6,7]. We attempted to use an x-ray streak camera during these tests to measure the duration of the x-ray bursts, since in principle the x-ray streak camera can have significantly higher temporal resolution than the single-shot oscilloscopes used to record data from PCDs. A 200  $\mu\text{m}$  wide slit was used in front of the photocathode of the streak camera, and a set of 12 different filters were placed along the slit direction to provide a continuous record of the x-ray emission in various spectral ranges. The filters used are identical to those described in previous work [24]. Most of the streak data obtained used a sweep rate of 1.143 ns/mm (speed 2), which covered a time window of roughly 40 ns. This sweep rate, combined with the slit width and internal magnification of the camera of about 1.2 resulted in a minimum time resolution in this configuration of about 0.25 ns. As such, its temporal resolution as used during these experiments was better than that of the PCDs.

The streak camera was not used during the first two experimental series. The camera was apparently damaged before or during the third experimental series, so that most of the streaks from that series were out of focus, with the exception of s3814 (the camera was refocused just before that shot). The camera electronics were sent out for repair before the 4<sup>th</sup> experimental series and there were no further issues with the electronics thereafter. The x-ray streak camera configurations for shots starting with s3814 are summarized in Table 9. To successfully field the streak camera without damaging the photocathode and/or the electronics required a fast-closing valve to stop debris and some Kapton baffling placed in the line of sight to shield from fast-moving gasses. To achieve the requisite vacuum near the streak camera photocathode we supplemented the SATURN chamber pumps with a local turbo pump. The electronics were all stored in a screen box immediately next to the streak camera. The hardware setup is depicted in the photos shown in Figure 22 and Figure 23.

There were four attempts to collect data with the streak camera's speed 3 (0.571 ns/mm) rather than speed 2. The first attempt on s3860 succeeded in collecting data but the other three returned blank films. We do not fully understand the timing of s3860, since the data on the streak does not appear to match up with the expected PCD signals. Based on our measurements of the required trigger delay when using speed 3, we also do not understand why we failed to get data on all three of the other shots. This slightly faster sweep rate would have provided us with still better time resolution. The estimated window center for each shot based on our understanding of the various trigger delays is summarized in Table 9.

In two experiments (s3865-s3866) we attempted to field the x-ray streak camera as part of a streaked x-ray spectrometer. This is discussed in more detail in the spectroscopy section.

**Table 9: Summary of x-ray streak camera (XRSC) diagnostic configurations and results.**

Shot	Mode	Streak Speed Mode	Estimated Window Center (ns)	Image Intens. gain	Image Intens. mode	Kapton baffle (microns)	Data on streak?
s3814	Slit	2	267	5	?	250	Yes
s3857	Slit	Focus	Focus	5	On	250	Yes
s3858	Slit	2	273	5	Fixed	250	No
s3859	Slit	2	265	3	On	250	Yes
s3860	Slit	3	256	5	Fixed	250	Yes
s3865	FASTR	Focus	Focus	5	?	125	Yes?
s3866	FASTR	2	257	6	Fixed	125	Yes?
s3895	Slit	3	258	5	Fixed	125	No
s3896	Slit	3	257	5	Fixed	125	No
s3897	Slit	2	265	5	Fixed	125	Yes
s3898	Slit	2	262	5	Fixed	125	No
s3899	Slit	3	260	5	Fixed	125	No
s3900	Slit	2	261	5	Fixed	125	Yes
s3940	Slit	2	272	5	Fixed	125	Yes
s3941	Slit	2	267	5	Fixed	125	No
s3942	Slit	2	264	5	Fixed	125	Yes
s3944	Slit	2	258	5	Fixed	125	Yes

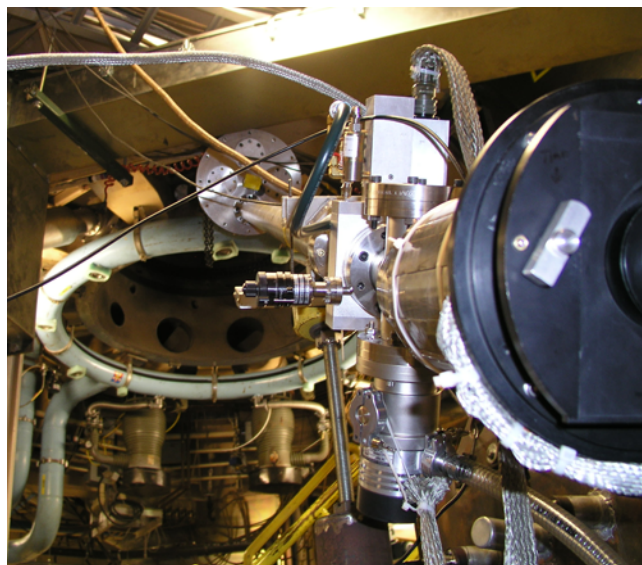


**Figure 22: View of SATURN vacuum chamber from the end of LOS C. The vacuum chamber ports can be seen inside the circular ring in the background. The connection point of LOS B can be seen to the upper left. The x-ray streak camera mounted on LOS C is seen in the foreground.**

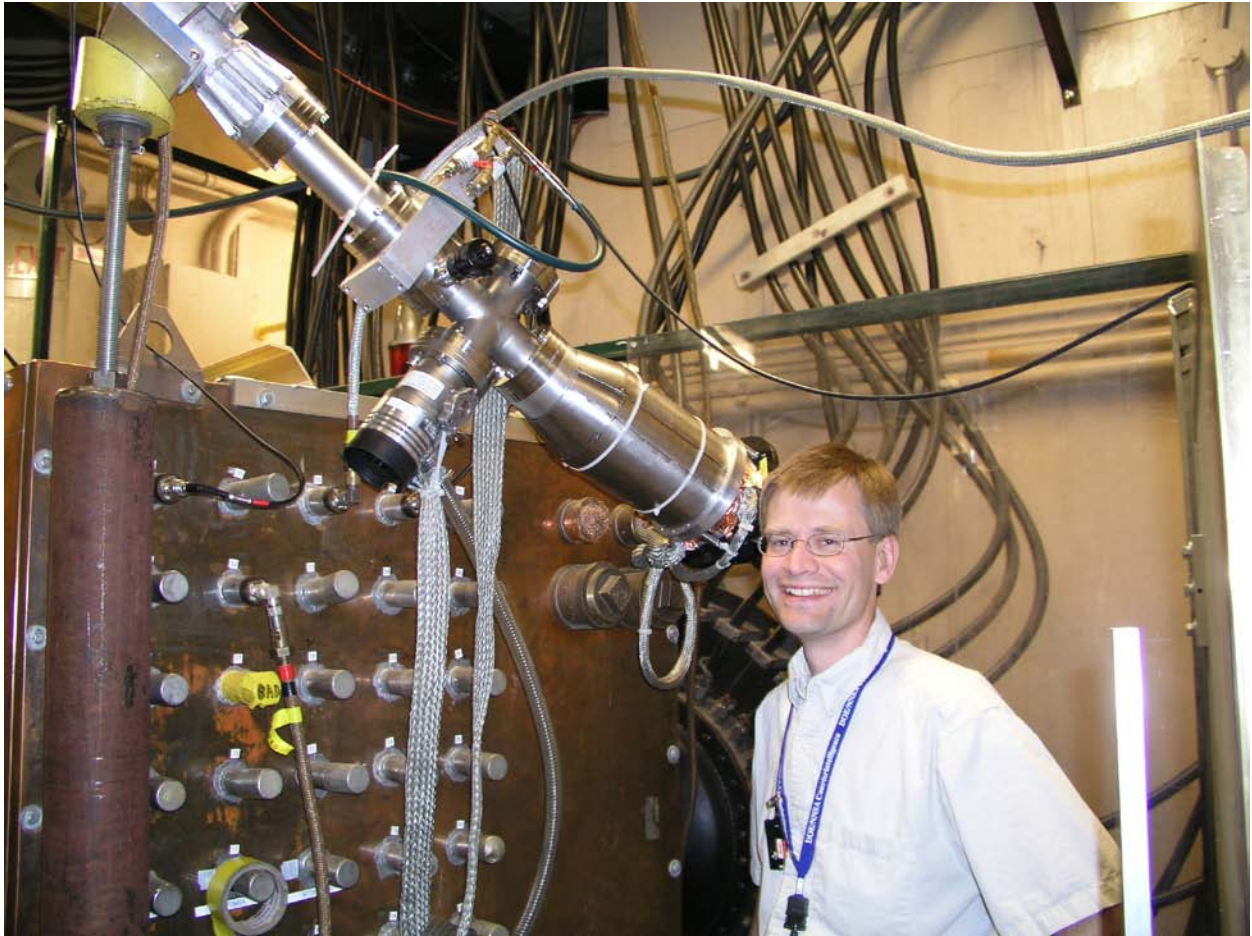


**Figure 23: Photo of the x-ray streak camera diagnostic as installed at the end of LOS C. A fast-closing valve was used at the end of the pipe to isolate the streak camera from debris and the post-shot rise in vacuum pressure. A polyimide filter was installed between the fast valve and turbo pump. An angle was placed just in front of the streak camera body to eliminate a direct line of sight down the pipe to the streak camera phosphor screen. The electronics controlling the streak camera and its micro-channel plate detector went through shielded cable into the large copper screen-box in the background. The streak camera body was shielded from magnetic fields using two pieces of mu-metal shielding held against the body by two white tie wraps. The author (DBS) is shown in the foreground.**

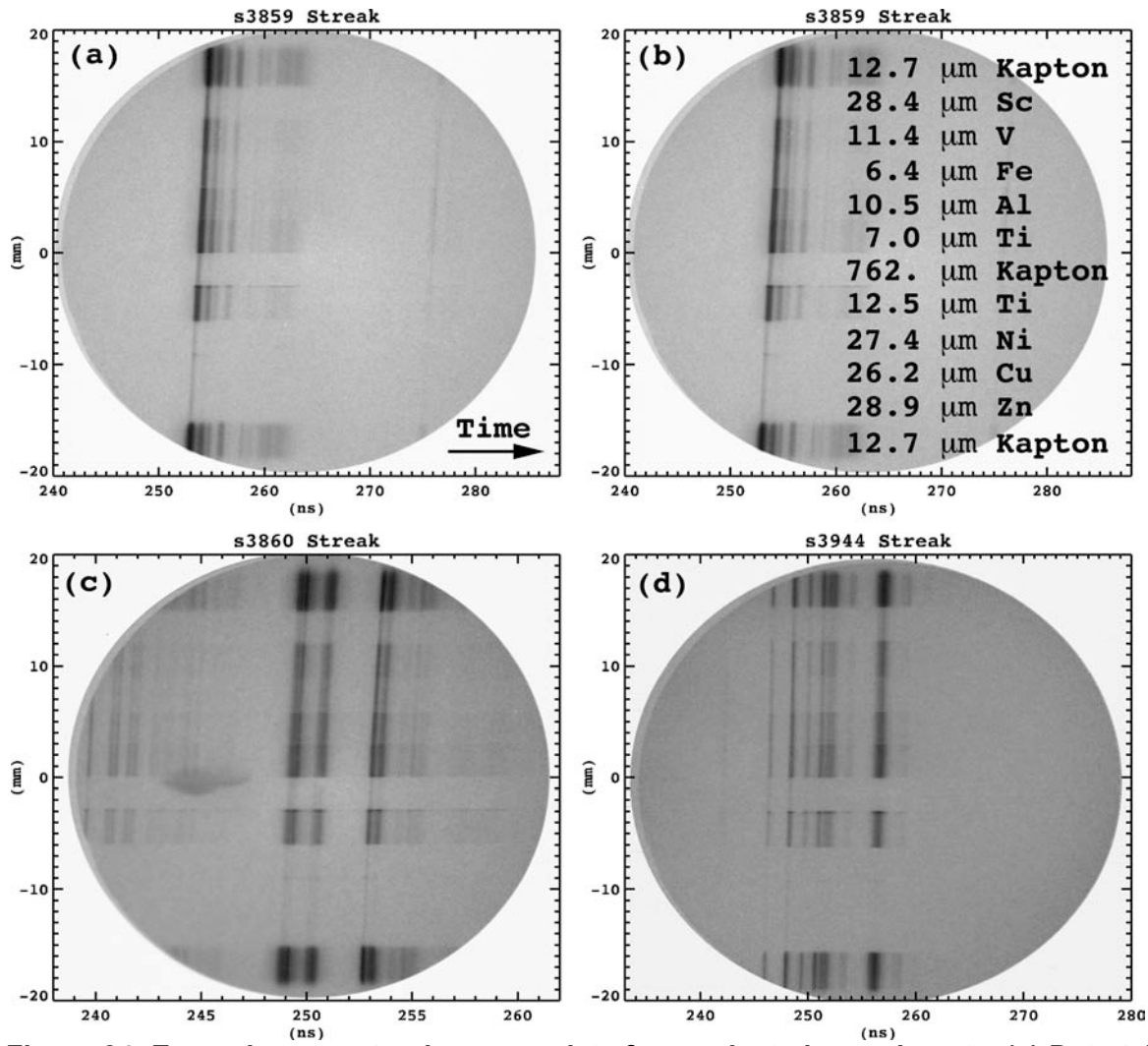


**Figure 24: Example x-ray streak camera data from selected experiments. (a) Data taken at speed 2 from s3859, a solid W/Cu X pinch, also shown in (b) with the 12 different filter labels superimposed over the image. (c) Data taken at speed 3 from s3860, a solid W/Cu X pinch. (d) Data taken at speed 2 from s3944, a solid W X pinch.**

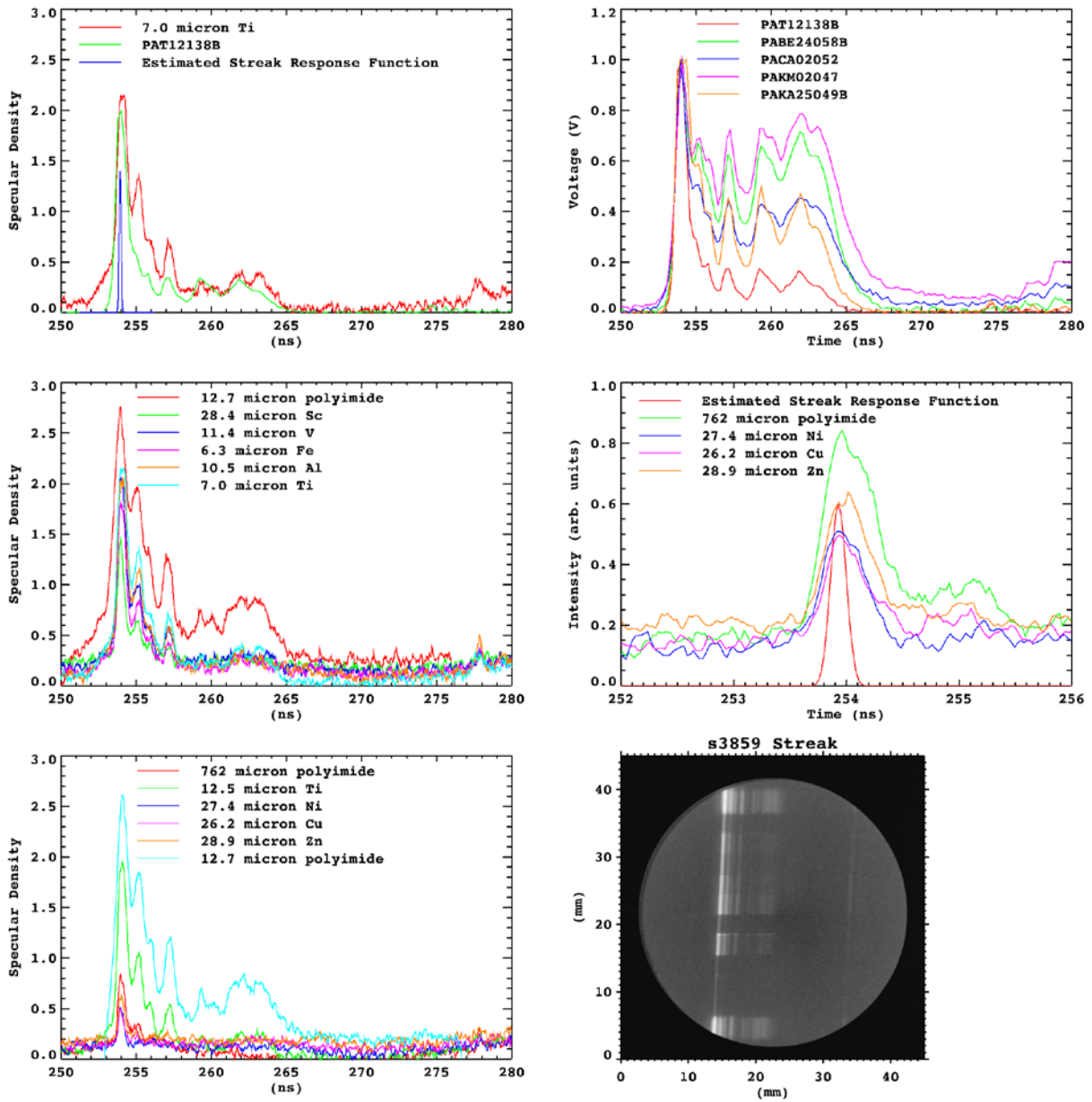


Figure 25: A comparison between the x-ray streak camera and PCD data from s3859, a solid W/Cu X-pinch load. The 7.0- and 12.5-micron Ti-filtered streak data fairly closely resembles the Ti-filtered PCD trace (signal PATi2138). The first x-ray burst in this experiment contained very hard radiation  $>6$  keV that was seen in the Ni-, Cu-, and Zn-filtered portions of the streak.

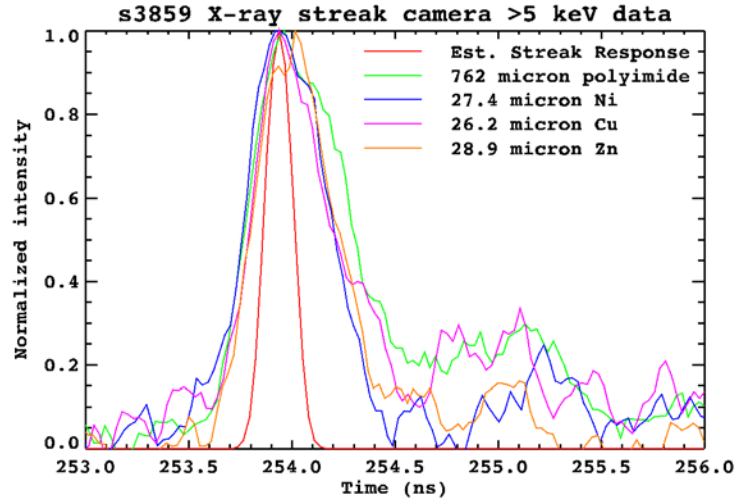


Figure 26: Hard (>6 keV) x-ray time duration from s3859 measured using the x-ray streak camera. Also shown in red is the estimated streak response function, estimated by convolving a 120-micron-wide square wave (the slit image) with a 100-micron FWHM Gaussian (representing the MCP spatial resolution). This is optimistic in that it assumes perfect focusing, which was not always maintained during the experiments. Subtracting the streak response function in quadrature gives FWHMs for the polyimide-, Ni-, Cu-, and Zn-filtered regions of 0.51, 0.42, 0.39, and 0.42 ns, respectively.

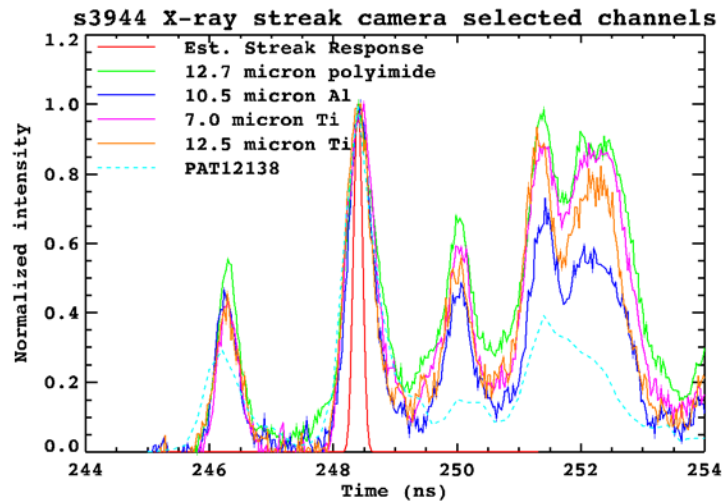


Figure 27: Selected streak camera lineouts compared with Ti-filtered PCD data from s3944, a solid W X-pinch load. The peak at 248.4 ns had FWHMs in the PCD and polyimide-, Al-, 7.0-micron Ti, and 12.5-micron Ti-filtered regions of 0.59, 0.44, 0.52, 0.47, and 0.56 ns, respectively.

### 3.3.5 X-ray spectroscopy measurements

One of our goals, assuming we were successful in creating relatively small x-ray sources, was to determine the plasma properties of those sources. This was done in the past for 0.2 MA experiments using x-ray spectroscopy, either using K-shell radiation or L-shell radiation. For this project, we created some targets out of alloys with the specific intention of trying to create useful x-ray spectra in the keV range. These alloys are summarized in Table 3.

The original plan was to field a time-integrated spectrometer to determine what spectra were present, and then ultimately to field a time-resolved spectrometer to measure the temporal variations in the spectra. The need for time-resolved spectra is based on previously published work at 0.2 MA, which showed that the continuum radiation associated with the smallest x-ray source sizes occurred first for 10-100 ps, and was followed by increasing levels of line radiation that came from both a larger area and over a longer period of time. Hence, it was felt that time-integrated spectra would not be sufficient to determine the plasma parameters.

The time-integrated measurements were made using a modified version of the time-integrated convex crystal (TIXTL) spectrometers fielded on the Z facility [25]. Those diagnostics are typically fielded at the end of a line-of-sight (LOS) pipe. In the SATURN experiments the TIXTL spectrometer box was placed inside the vacuum chamber mounted to a flat-plate shield containing the imaging slits. A photograph of the TIXTL box can be seen in Figure 16.

The TIXTL used a LIF 200 crystal (2d spacing of 4.027 Angstroms), bent in a convex cylindrical shape with a radius of 1". The crystal was not rotated at all (zero degree rotation.) Two imaging slits with different widths were used at the entrance to the TIXTL box to be able to span a wide dynamic range. Some beryllium and Kapton filters were also placed over the entrance to the TIXTL box or in front of the slits to protect them. The source-to-slit distance was 233 mm, and the slit-to-crystal distance was another 81 mm beyond that. Generally we used x-ray sensitive films as the detectors (Kodak 2492, 2497, or DR-50). On one experiment we attempted to use imaging plate, but the entire plate was completely saturated even after 7 scans. This is because of the very high-energy background flux seen inside the SATURN vacuum chamber. The TIXTL box was only made of aluminum, and did not therefore offer much shielding against the 0.01-1 MeV x rays that image plate is designed to detect. The TIXTL was not fielded until the third experimental shot series on SATURN, and was also not fielded during the final shot series (pure tungsten spectra are generally too difficult to work with). A summary of the TIXTL configurations used is found in Table 10.

On two shots (s3865-s3866) during fourth experimental series the we attempted to field a time-resolved spectrometer. The spectrometer geometry was that of a focusing spectrograph with spatial resolution (FSSR). The hardware used was from the so-called "FASTR" diagnostic originally built for the Z facility [26], and the distances were very similar. For the large distance to the crystal used (~6.6 m) and the expected sub-mm source size, the spatial extent of the spectrum would be below the spatial resolution of the streak camera, making it equivalent to a slit image. The design configuration used on the two shots turned out to be incorrect for capturing Cu K-shell spectra, as shown by subsequent offline testing using a Manson source.

Given the complexity of fielding the instrument and the relative lack of direct x-ray streak camera data, it was decided not to field the instrument during the fifth experimental series and to focus instead on getting more direct streak data. The targets fielded during the sixth and final experimental series on SATURN were all pure tungsten targets and not interesting from a spectroscopic viewpoint, so the instrument was not fielded then either. It may be possible to capture Ni and or Cu K-shell radiation during a future experiment using this diagnostic on SATURN.

**Table 10: Summary of TIXTL configurations and data.**

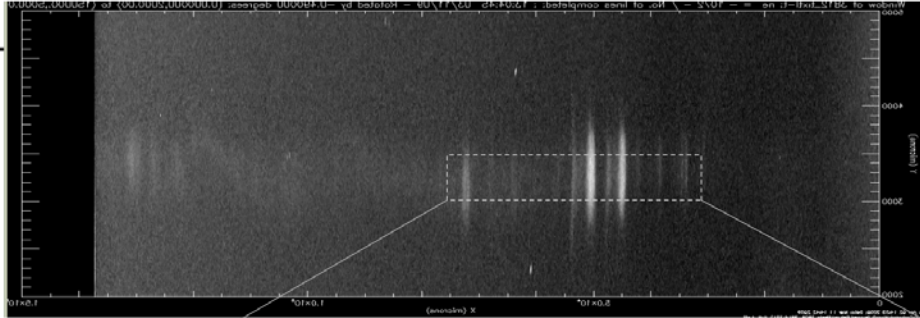
Shot	Slit widths (microns)	Films	Filters (microns)	Data notes
3808	300/100	TR image plate	25 Be + 100 Kapton	Saturated
3809	300/100	2492, 2492	25 Be + 100 Kapton	OK, film loaded incorrectly
3810	200/50	2492, 2492	25 Be + 150 Kapton	Faint lines + continuum
3811	300/100	2497, 2492	25 Be + 200 Kapton	Faint lines + continuum
3812	300/100	2497, 2492	25 Be + 200 Kapton	Good
3814	300/100	2497, 2492	25 Be + 200 Kapton	Good
3857	300/100	2497, 2492	25 Be + 200 Kapton	Mainly lines with little continuum
3858	300/100	2497, 2492	25 Be + 200 Kapton	Good
3859	300/100	2497, 2492	25 Be + 200 Kapton	Faint lines + continuum
3860	300/100	2497, 2492	25 Be + 200 Kapton	Faint lines + continuum
3865	300/100	2497, 2492	25 Be + 200 Kapton	OK, but lost low-energy data
3866	300/100	2497, 2492, DR-50	25 Be + 200 Kapton	Good
3895	200/50	2497, 2492, DR-50	25 Be + 200 Kapton	Weak
3896	200/50	2497, 2492, DR-50	25 Be + 200 Kapton	Weak
3897	200/50	2497, 2492, DR-50	25 Be + 200 Kapton	Good
3898	200/50	2497, 2492, DR-50	25 Be + 200 Kapton	Continuum
3899	200/50	2497, 2492, DR-50	25 Be + 200 Kapton	No data
3900	200/50	2497, 2492, DR-50	25 Be + 200 Kapton	Good

The data from the TIXTLs has not yet been analyzed in detail yet. As people familiar with x-ray spectroscopy are aware, there are many potential pitfalls in the data analysis and the utility of analyzing time-integrated spectra may be relatively low. A preliminary analysis of one of the earliest shots (s3812) with a Cu/Ni/Mn target was done for the 2009 Wire Array Workshop and is shown in Figure 28. More analysis of this data can be done in the future using the PRISMSPECT set of tools to better estimate the parameters.



# Quick analysis of time-integrated K-shell spectra from Cu/Ni X pinch shows hot plasma

s3812  
CuNi



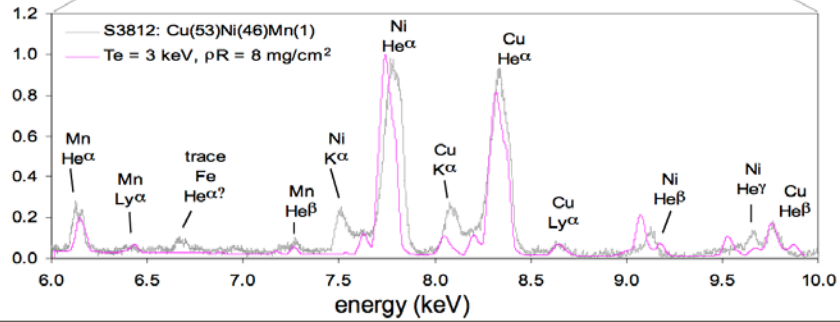
**First cut diagnostics:**

Estimate  $\rho R$  by fitting Mn/Ni He $\alpha$  ratio

Estimate Te by fitting Ly $\alpha$ /He $\alpha$  ratios

Poor fit above 9 keV

Temperature gradients evidenced by cold K $\alpha$  features



K-shell size  $>10 \mu\text{m}$  ( $\sim 50 \mu\text{m}$ ?), so density  $\sim 1.6 \text{ g/cc}$ ?? More work needed

Figure 28: Example TIXTL data from s3812 (Cu/Ni/Mn target) and a preliminary analysis.

## 4. DISCUSSION OF KEY EXPERIMENTAL RESULTS

As discussed in Section 2, the main project challenges were:

1. Determine if and how micropinch plasmas driven by 4-6 MA could be created; and
2. To diagnose the conditions of any resulting micropinch plasmas.

The project succeeded in finding a load configuration that was capable of creating micropinch plasmas with extreme conditions. Some of the parameters investigated during the course of the project included:

- a. The project tested several materials and alloys (W, Mo, Ni/Cr, Cu/Ni/Mn, and W/Cu). Of these, the pure tungsten and W/Cu alloys appeared to generate the smallest x-ray spots and gave the highest radiation power/energy. Tungsten was the highest-Z material tested, and this trend may suggest radiation loss is critical to achieving small radiation sources at high currents. We note that molybdenum was only tested once in a non-optimal configuration, so it remains unclear whether a mid-Z material like Mo can perform as well as tungsten.
- b. The project tested wire-based X pinches composed from a single wire array and nested wire arrays. It also tested “solid” X pinches made from a single, machined cross-point. The latter were easy to field generated some of the best results of this project. The solid X-pinch target geometry should also scale well to higher currents than 3-6 MA.
- c. A criterion for the scaling of the X-pinch mass per unit length and minimum diameter with increasing current and rise was developed based on the dimensionless scaling of Ryutov et al. [27].

The project succeeded in diagnosing some of the parameters of X-pinch plasmas, including:

- a. A time-integrated slit-imaging camera was developed to measure the source size of >4 keV continuum x rays emitted by X pinches. A source size of 5-7 microns was measured in at least one experiment.
- b. The power and energy radiated by X pinches was diagnosed using x-ray diodes, photo-conducting diodes, and bolometers. Many loads produced bright and compact (~3 mm diameter) sources of soft (0.1-1.0 keV) x rays that radiated ~4 TW/mm and >60 kJ/mm.
- c. An x-ray streak camera diagnostic was developed to measure the time duration of the >4 keV x-ray emission. Many of the loads produced >6 keV continuum x-ray sources with durations <0.5 ns.
- d. A time-integrated x-ray spectrometer was fielded on shots containing Cu, Ni, and/or Mn dopants and time-integrated plasma temperatures of 2-3 keV were evident. Clear evidence for Cu K-shell radiation at >8 keV was seen from a region a few hundred microns in size.

The project did not succeed in making time-resolved spectroscopic measurements of the plasma parameters of a micropinch. This was an ambitious goal, and though attempts were made to field a streak x-ray spectrometer during the course of the project, we did not succeed in the time frame allotted to the project.



## 5. PROJECT ACCOMPLISHMENTS

Some of the accomplishments of this project include:

(1) We developed a criterion that could be used to estimate the mass/length and diameter scaling of an X pinch to currents  $>1$  MA.

(2) We found an optimum load geometry (the “solid” X pinch) that gave good data for high-current X-pinch experiments in the 3-6 MA range, which can also be readily scaled to higher currents as needed.

(3) We partially optimized the specific X-pinch parameters of a solid X-pinch target made of tungsten, and succeeded in generating micropinch plasmas.

(4) We made an initial diagnosis of X-pinch and micropinch parameters on our 3-6 MA experiments, summarized as follows:

- a. Sources of  $>6$  keV continuum x rays that were 5-10 microns in size and  $<500$  ps in duration
- b. Time-integrated plasma temperatures of 2-3 keV capable of making Cu K-shell radiation from relatively compact (few hundred microns) x-ray sources
- c. Bright and compact ( $\sim 3$  mm) sources of soft (0.1-1 keV) x rays  $\sim 4$  TW/mm and  $>60$  kJ/mm

(5) SATURN and related work at 1 MA COBRA facility at Cornell University has led to a number of scientific publications in refereed journals, and at least one more publication on the SATURN results should be submitted before the end of 2010;

- a. “Symmetric multilayer MegaAmpere X-pinch,” T.A. Shelkovenko, S.A. Pikuz, R.D. McBride, P.F. Knapp, G. Wilhelm, D.B. Sinars, D.A. Hammer, and N. Yu. Orlov, Plasma Physics Reports 36, 50-66 (2010).
- b. “Nested X pinches on the COBRA generator,” T.A. Shelkovenko, S.A. Pikuz, R.D. McBride, P.F. Knapp, H. Wilhelm, D.A. Hammer, D.B. Sinars, AIP Conf. Proc. 1088, 155 (2009).
- c. “Nested multilayered X pinches for generators with mega-ampere current level,” T.A. Shelkovenko, S.A. Pikuz, R.D. McBride, P.F. Knapp, H. Wilhelm, D.A. Hammer, and D.B. Sinars, Physics of Plasmas 16, 050702 (2009).
- d. “Bright spots in 1 MA X pinches as a function of wire number and material,” D.B. Sinars, S.A. Pikuz, J.D. Douglass, R.D. McBride, D.J. Ampleford, P. Knapp, K. Bell, D. Chalenski, M.E. Cuneo, J.B. Greenly, D.A. Hammer, B.R. Kusse, A. Mingaleev, T.A. Shelkovenko, and D.F. Wenger, Phys. Plasmas 15, 092703 (2008).

(6) Newly hired experimenters in the inertial confinement fusion research group (McBride, Harding) were able to obtain hands-on experience working on x-ray instrumentation and large-scale pulsed power at Sandia prior to their first Z experiments.



## 6. IDEAS FOR FUTURE WORK

After some additional analysis, we are planning to publish some of the key experimental results of the SATURN experiments described in this report, which represent an advancement of the state-of-the-art of X-pinch research. There remain several opportunities for the future.

Some possibilities for future work beyond the conclusion of this project are suggested below.

(1) Continuation of SATURN X-pinch scaling work as part of new-hire LDRD program. The SATURN facility is extremely flexible and requires a significant amount of hands-on labor and fielding of diagnostics on the part of the principal experimenters. As such, it can be an excellent training facility for new hires, particularly those who would benefit from more experience with x-ray instrumentation and pulsed power. The physics of X pinches is fundamentally concerned with understanding the practical limits of the use of the JxB force to compress materials. This physics is central to all of the research being done on pulsed power facilities, and as such it is also an appropriate source of physics training for new hires who may have limited experience with z-pinch physics. Some specific project goals could include:

- a. Further optimization of X-pinch load parameters, particularly with an eye toward obtaining x rays closer to peak current with presumably more extreme conditions and possibly fewer x-ray bursts overall.
- b. Time-resolved x-ray spectroscopy, possibly using a streaked focusing spectrometer with spatial resolution (FSSR) as originally intended during this project. This would allow the determination of plasma parameters without relying on time-integrated spectrometers.
- c. Using 2-3 X-pinch cross points at the load of the SATURN facility. Experience on 0.2-1 MA facilities suggests that X pinches work better and more reliably in parallel.
- d. Imaging of the X-pinch cross point with 10-100 micron spatial resolution. This is required to demonstrate that the plasma points are the result of magnetic compression.

(2) Scaling of SATURN results to ~10 MA version of Z as part of Z Basic Science program. Staff scientists at both Cornell University and UCSD have expressed some interest in this possibility. In addition to the possibility of more extreme parameters, the principal benefit would be the ability to take advantage of the existing (and permanent) diagnostic suite at Z. This diagnostic suite includes some diagnostics unavailable at SATURN, such as x-ray radiography using the Z-Beamlet laser. Developing and fielding complex diagnostics such as time-resolved spectrometers would also be easier as they already exist and/or could be established on quasi-permanent lines of sight.

(3) Use of X-pinch loads in repetition-rate experiments on 1-MA MYKONOS facility. Solid X-pinch loads developed for SATURN and subsequently tested on the 1-MA COBRA facility at Cornell University are robust and very easy to install quickly. As such, they may be interesting z-pinch loads for future rep-rate pulsed power demonstrations in coming years rather than just firing into a short circuit load.

[This page intentionally left blank]

## 7. PROJECT SIGNIFICANCE AND CONCLUSIONS

This project addressed the fundamental physics of magnetically driven implosions using X-pinch targets. What are the ultimate limits for the magnetic compression of plasma using the JxB force? What are the most extreme plasma conditions we can create in the laboratory using magnetic compression? This physics is of significant programmatic interest to Sandia, since most research using pulsed power drivers relies on the JxB force to move, shock, and/or compress material to the extreme conditions required for stockpile stewardship research.

This project represents a first step down a path toward understanding the limits of magnetic compression at currents >1 MA. The project was primarily a survey of high current (3-6 MA) X pinches to understand whether extreme plasma conditions might be occurring in the laboratory. The project succeeded in creating x-ray sources that appear to be interesting and potentially worthy of future study.

Though it was not the primary goal of the project, we note that several X-pinch loads produced ~10 TW and ~190 kJ of soft (0.1-1 keV) x-rays from a diameter of ~3 mm. This corresponds to about 4 TW/mm and about 60 kJ/mm from a ~6 MA current generator. For comparison, the published power and yield from tungsten wire arrays on SATURN by Deeney et al. [29] was 75+/-10 TW and 450+/-50 kJ from a 20 mm pinch length, or about 4 TW/mm and 23 kJ/mm. Tungsten wire arrays on Z (40 mm diameter, 20 mm tall) produced ~240 TW and ~1800 kJ, which corresponds to ~12 TW/mm and ~90 kJ/mm. In other words, the radiation power and energy created at stagnation in the X-pinch loads was comparable to those created in wire-array z-pinches. The two approaches are different, however, in that the wire arrays relied on a high-velocity implosion to reach extreme conditions, whereas in the X pinch all of the mass started on the axis from the beginning. That is, the X pinch does not rely on the conversion of magnetic energy into kinetic energy and thereafter to radiation energy, at least not in the traditional way. Rather, it relies on the steady application of the JxB force to plasma on the axis in a way that continuously does work and ultimately compresses at least a small fraction of the plasma to extremely small diameters.

How tight a radius does the current achieve? We can only speculate at this point, but we believe that the potential that extreme conditions were achieved on SATURN is very high. Consider that in at least one experiment we created a bright >6 keV x-ray source from a tungsten plasma that was 5-7 microns in diameter, or ~3 microns in radius. If one assumes that ~3 MA was flowing at that radius, it would correspond to a magnetic pressure of  $140 \cdot (3/30)^2 / (3e-3 \text{ mm})^2$  Mbar, or over 150 Gbar! Even if only 0.3 MA of current made it to that radius, the pressure would still have been 1.5 Gbar. For reasonable plasma temperatures of 0.6-3 keV, these pressures correspond to ion densities in excess of solid density. The ultimate goal of the community's research into the limits of magnetically driven systems should be to determine if it is possible to directly use magnetic pressure to achieve extreme material conditions and, if possible, exploit this possibility for the betterment of humanity.

At this time we are still analyzing the data in detail to determine what defensible and less speculative conclusions can be made, at which time we will submit a manuscript to a refereed physics journal describing this research.

## REFERENCES

1. D. Mosher *et al.*, Appl. Phys. Lett. 23, 429 (1973).
2. P.G. Burkhalter *et al.*, Phys. Rev. A 15, 700 (1977).
3. S.M. Zakharov *et al.*, Sov. Tech. Phys. Lett. 8, 456 (1982).
4. B.M. Song *et al.*, Appl. Optics 44, 2349 (2005).
5. T.A. Shelkovenko *et al.*, Rev. Sci. Instrum. 72, 667 (2001).
6. S.A. Pikuz *et al.*, Phys. Rev. Lett. 89, 035003 (2002).
7. D.B. Sinars *et al.*, J. Quant. Spectrosc. Radiat. Transf. 78, 61 (2003).
8. S.B. Hansen *et al.*, Phys. Rev. E 70, 026402 (2004).
9. S.A. Pikuz *et al.*, Proc. SPIE 4504, 234 (2001).
10. F.N. Beg *et al.*, Appl. Phys. Lett. 89, 101502 (2006).
11. J.P. Chittenden *et al.*, Phys. Rev. Lett. 98, 025003 (2007).
12. T.A. Shelkovenko *et al.*, IEEE Trans. Plasma Sci. 34, 2336 (2006).
13. T.A. Shekovenko *et al.*, Rev. Sci. Instrum. 77 (2006).
14. X.B. Zou *et al.*, Laser and Particle Beams 24 (2006).
15. L.E. Aranchuk *et al.*, Journal De Physique IV 138 (2006).
16. G.A. Chandler *et al.*, Rev. Sci. Instrum. 70, 561 (1999).
17. D.L. Fehl *et al.*, Rev. Sci. Instrum. 71, 3072 (2000).
18. R.B. Spielman *et al.*, Rev. Sci. Instrum. 70, 651 (1999).
19. R.B. Spielman *et al.*, Rev. Sci. Instrum. 68, 782 (1997).
20. R.B. Spielman *et al.*, Rev. Sci. Instrum. 66, 867 (1995).
21. B. Jones *et al.*, Rev. Sci. Instrum. 75, 4029 (2004).
22. B. Jones *et al.*, Rev. Sci. Instrum. 77, 10E316 (2006).
23. B. Jones *et al.*, Rev. Sci. Instrum. 79, 10E906 (2008).
24. D.B. Sinars *et al.*, Phys. Plasmas 15, 092703 (2008).
25. T.J. Nash *et al.*, Rev. Sci. Instrum. 72, 1167 (2001).
26. D.B. Sinars *et al.*, Rev. Sci. Instrum. 77, 10F327 (2006).
27. Ryutov, Derzon, and Matzen, Rev. Mod. Phys. 72, 167 (2000).
28. T.A. Shelkovenko *et al.*, Phys. Plasmas 16, 050702 (2009).
29. C. Deeney *et al.*, Phys. Rev. E, 5945 (1997).

## DISTRIBUTION

1 Prof. J.P. Chittenden  
Blackett Laboratory, Imperial College  
London SW7 2BW, United Kingdom

2 Dr. Sergei A. Pikuz  
Laboratory of Plasma Studies, Cornell University  
Ithaca, New York 14853, USA

1 MS1193 Daniel B. Sinars Org. 1643

1 MS1193 Ryan D. McBride Org. 1643

1 MS1193 Michael E. Cuneo Org. 1643

1 MS0899 Technical Library 9536 (electronic copy)

For LDRD reports, add:

1 MS0359 D. Chavez, LDRD Office 1911



**Sandia National Laboratories**